Mon. Not. R. Astron. Soc. **000**, 000–000 (0000) Printed 1 February 2008 (MN LATEX style file v1.4)

The Las Campanas/AAT Rich Cluster Survey: II. The Environmental Dependance of Galaxy Colours in Clusters at z∼0.1.

Kevin A. Pimbblet,[1] Ian Smail,[1] Tadayuki Kodama,[2,1] Warrick J. Couch,[3] Alastair C. Edge,[1] Ann I. Zabludoff[4] & Eileen O'Hely[3]

[1] *Department of Physics, University of Durham, South Road, Durham, DH1 3LE, UK*
[2] *Department of Astronomy, University of Tokyo, Hongo, Bunkyo-ku, Tokyo, 113-0033, Japan*
[3] *School of Physics, University of New South Wales, Sydney NSW 2052, Australia*
[4] *Steward Observatory, University of Arizona, Tucson AZ 85721 USA*

Accepted ... ; Received ... ; in original ...

ABSTRACT

We present a photometric investigation of the variation in galaxy colour with environment in 11 X-ray luminous clusters at $0.07 \leq z \leq 0.16$ taken from the Las Campanas/AAT Rich Cluster Survey. We study the properties of the galaxy populations in individual clusters and take advantage of the homogeneity of the sample to combine the clusters together to investigate weaker trends in the composite sample. We find that modal colours of galaxies lying on the colour-magnitude relation in the clusters become bluer by $d(B-R)/dr_p = -0.022 \pm 0.004$ from the cluster core out to a projected radius of $r_p = 6\,\mathrm{Mpc}$; further out in radius than any previous study. We also examine the variation in modal galaxy colour with local galaxy density, Σ, for galaxies lying close to the colour-magnitude relation and find that the median colour shifts bluewards by $d(B-R)/d\log_{10}(\Sigma) = -0.076 \pm 0.009$ with decreasing local density across three orders of magnitude. We show that the position of the red envelope of galaxies in the colour-magnitude relation does not vary as a function of projected radius or density within the clusters, suggesting that the change in the modal colour results from an increasing fraction of bluer galaxies within the colour-magnitude relation, rather than a change in the colours of the *whole* population. We show that this shift in the colour-magnitude relations with projected radius and local-density is greater than expected from the changing morphological mix based on the local morphology–density relation. We therefore conclude that we are seeing a real change in the properties of galaxies on the colour-magnitude relation in the outskirts of clusters. The simplest interpretation of this result (and similar constraints in local clusters) is that an increasing fraction of galaxies in the lower density regions at large radii within clusters exhibit signatures of star formation in the recent past, signatures which are not seen in the evolved galaxies in the highest density regions.

Key words: surveys, catalogues, galaxies: photometry, galaxies: clusters: general, galaxies: clusters: individual: A 22, A 550, A 1079, A 1084, A 1285, A 1437, A 1650, A 1651, A 1664, A 2055, A 3888.

1 INTRODUCTION

Visvanathan and Sandage (1977) first noted that the more luminous early-type galaxies (ellipticals and S0s) within Coma and eight other local clusters exhibit systematically redder integrated colours than the late-types. These galaxies also demonstrate a tight correlation between their colours and magnitudes: the colour-magnitude relationship (CMR; e.g. Bower, Lucey and Ellis 1992). Kodama & Arimoto (1997) show that the slope of the colour-magnitude relation is primarily due to the mean stellar metallicity (as suggested by Dressler 1984), while the scatter around the relation may be due to age effects (Kodama et al. 1999).

As one moves from the cores of clusters into the surrounding field the morphological mix in the galaxy population shifts from almost completely passive, early-types to

one dominated by star-forming spiral galaxies. This is the origin of the Morphology-Density relation (T–Σ; Dressler 1980). The environmental "transition" region between clusters and the field is an important region to study if we are to learn what impact environment has on galaxy properties such as star formation rate, luminosity and morphology. Recent numerical simulations of clusters of galaxies show that the history of galaxy accretion is retained in the cluster's radial profile. The first galaxies to be accreted still reside nearer the centre while more recent additions are located preferentially on the outskirts of clusters (Diaferio et al. 2001). This means that if the star formation in galaxies is suppressed when they enter the cluster environment (Balogh, Navarro & Morris 2000), then the variation in the typical accretion age of cluster galaxies with radius may be visible in the ages of the stellar populations of the passive cluster members which inhabit the colour-magnitude relation. Studies of galaxies in the outskirts of clusters and the variation in their properties with redshift can therefore inform us about whether environment has altered the characteristics of cluster galaxies as the clusters have been assembled over the Hubble time.

There are two main observational techniques to trace the variation in the stellar populations of galaxies between the field and cluster and its evolution with redshift: photometry and spectroscopy.

Wide-field photometric studies of clusters have uncovered evidence of changes in the colours of the galaxy populations with radius: Butcher & Oemler (1978, 1984) first identified a photometric radial gradient; the fraction of blue galaxies increases with projected distance, out to $\sim 1.5\,\mathrm{Mpc}^{\star}$ (as well as increasing dramatically with redshift). Kodama & Bower (2000) confirm this strong trend in their recent photometric study of the intermediate redshift clusters from the CNOC survey (Yee et al. 1996). Such trends of average colour with environment (i.e. radius or local density) could be due to (i) a systematic, intrinsic cluster colour gradient in one or both of the dominant elliptical and S0 populations of the CMR with environment; or (ii) be primarily driven by the morphology-density relation (Dressler 1980), where the late-type to early-type galaxies ratio is a strongly decreasing function of local galaxy density, or equivalently an increasing function of clustocentric distance (Whitmore & Gilmore 1991). Thus the observed trend may simply reflect evolution in the morphological mix, rather than representing changes in the colours of the galaxies lying on the CMR with environment (as we discuss below, variations in the morphological mix *within* the CMR may produce more subtle changes in colour with environment).

To reliably differentiate between these options we need to compare the properties of morphologically-selected (or, failing, that colour-selected) early-type galaxies in the outskirts of clusters with similar galaxies in the high density cores. In this way we can determine if the blueing trend occurs in the passive cluster population or simply reflects an increasing proportion of late-type galaxies.

Unfortunately, very few of the existing studies of clusters have the field of view, photometric precision (the expected colour shifts are $\lesssim 0.10$ mags) or colour information necessary to investigate the possible variation with environment of the colour of the galaxies on the CMR. One of the few relevant studies is the recent investigation by Terlevich et al. (2001) of the $(U-V)$ colours of ~ 100 morphologically-classified early-type galaxies across a 1.5° field within the Coma cluster ($z = 0.023$). They identify a trend for the colours of early-type galaxies to be systematically bluer at a fixed luminosity outside the core of the cluster. They interpret this as a result of age differences and suggest that there is a 2 Gyr difference between the mean luminosity-weighted ages of the stellar populations of galaxies in the core and those outside 0.5 Mpc.

At higher redshifts, deep multi-colour imaging with *Hubble Space Telescope* (*HST*) of distant clusters has sufficient sensitivity to uncover the signs of the variation in the CMR with environment, as well as providing detailed morphological information which can be used to remove the effects of changes in the morphological mix from the analysis (Ellis et al. 1997). However, the limited field of view of the *WFPC2* camera means that these *HST*-based surveys are restricted to the inner regions of clusters. For example, van Dokkum et al. (1998) discuss the radial dependence of the CMR for the distant cluster MS 1358+62 at $z = 0.33$ within a ~ 1.6 Mpc region. They find no radial dependence of the zero-point of the CMR, or the scatter around it, for bulge-dominated galaxies at any radius. They do find, however, an increasing scatter around the CMR for early-type disk galaxies in the outer parts of their survey region (van Dokkum et al. 2000). They propose that this trend is caused by infalling galaxies at the outskirts of the cluster, but the absence of detailed morphological classifications for the early-type disk galaxies still leaves open the possibility that their result may again be due to subtle changes resulting from the morphology-density relation.

Spectroscopy provides a much more sensitive tool to investigate the variation in the ages of the stellar populations of galaxies with environment, as well as providing unambiguous membership information for galaxies at large projected distances from the cluster centre. Spectral signatures of past activity can remain measurable for ∼2 Gyrs after the star formation has ceased, by which time the photometric signatures may have become undetectable (e.g. Terlevich et al. 1999). Spectroscopic surveys of both local and distant clusters have uncovered precisely these signatures: identifying a class of galaxies with spectral features (enhanced Balmer absorption lines) indicative of recently ended star formation (Couch & Sharples 1987; Caldwell et al. 1993). The galaxies are classified as a+k or k+a based on the strength of the Balmer absorption lines (Dressler et al. 1999), equivalent terms are E+A, PSG and HDS (Couch & Sharples 1987). Global gradients in these spectral indices have been identified in galaxies from a sample of X-ray selected distant clusters (Balogh et al. 1999). However, the samples available from most spectroscopic studies are relatively modest and for the most part lack detailed morphological information. Thus there is a similar ambiguity to that in the analysis of the photometric gradient, due to the morphology-density relation, and it is difficult to interpret the origin of the radial gradients observed in key spectroscopic emission line indicators (Poggianti et al. 1999).

One survey which combines the photometric and spec-

* Throughout this work values of $H_0 = 50$ km s^{-1} Mpc^{-1} and $q_o = 0.5$ have been adopted.

Table 1. Details of the clusters from the LARCS sample used in this work. For each cluster we give the coordinates of the cluster centre, the redshift (z) and its X-ray luminosity, L_X, in the 0.1–2.4 keV passband (Ebeling et al. 1996). We also list the parameters of the biweight fit to the CMR within 2 Mpc of the centre of each of the clusters as plotted in Figure 1. The slope, colour at the fiducial magnitude and associated errors are taken from the median of 100 realizations of the background subtraction. These errors may be underestimated due to the way in which the CMR is fitted (see text for details). The apparent R-band magnitude corresponding to our fiducial absolute magnitude of $M_V = -21.8$ is also given for each cluster. The colour of each CMR at a fiducial magnitude equivalent to $M_V = -21.8$ and the slope of the relationship are examined as a function of redshift in Figure 2.

Cluster	R.A. (J2000)	Dec.	z	L_X (10^{44}erg s^{-1})	Slope	$(B-R)_{M_V=-21.8}$	$R_{M_V=-21.8}$
A 22	00 20 38.64	−25 43 19	0.131	5.31	-0.054 ± 0.008	1.85 ± 0.08	17.12
A 550	05 52 51.84	−21 03 54	0.125	7.06	-0.057 ± 0.006	2.05 ± 0.07	17.01
A 1079 ‡	10 43 24.90	−07 22 45	0.132	<0.45	-0.045 ± 0.003	1.80 ± 0.05	17.14
A 1084	10 44 30.72	−07 05 02	0.134	7.42	-0.051 ± 0.009	1.83 ± 0.06	17.17
A 1285	11 30 20.64	−14 34 30	0.106	5.47	-0.056 ± 0.014	1.87 ± 0.13	16.61
A 1437	12 00 25.44	+03 21 04	0.133	7.72	-0.072 ± 0.005	1.94 ± 0.12	17.15
A 1650	12 58 41.76	−01 45 22	0.084	7.81	-0.039 ± 0.003	1.69 ± 0.06	16.06
A 1651	12 59 24.00	−04 11 20	0.084	8.25	-0.047 ± 0.003	1.63 ± 0.08	16.06
A 1664	13 03 44.16	−24 15 22	0.127	5.36	-0.060 ± 0.015	1.73 ± 0.13	17.05
A 2055	15 18 41.28	+06 12 40	0.102	4.78	-0.052 ± 0.013	1.70 ± 0.08	16.53
A 3888	22 34 32.88	−37 43 59	0.151	14.52	-0.097 ± 0.017	2.12 ± 0.16	17.47

(‡) Although not originally fulfilling the LARCS selection criteria, A 1079 resides in the field of A 1084 at a similar redshift to the latter and is thus included in this study.

troscopic techniques is the study of A 2390 ($z = 0.23$) by Abraham et al. (1996). They combine a large spectroscopic survey covering a wide field (to provide spectral line indices and membership) and precise photometry. They demonstrate that the colours of the reddest spectroscopically-confirmed cluster members on the colour-magnitude relation become progressively bluer as a function of clustocentric distance out to 5 Mpc, a trend which was also seen in Balmer line indices. They interpret these radial gradients as arising from a decrease in the mean luminosity-weighted age of the stellar populations in galaxies at larger projected distances from the cluster's centre. They suggest that this results from the truncation of star formation as galaxies and groups are accreted from the field onto the cluster outskirts, building up the cluster in an "onion-ring" fashion reminiscent of the hierarchical picture of cluster formation (Lacey & Cole, 1993; Cole et al. 2000).

The impressive studies of Coma by Terlevich et al. (2001) and A 2390 by Abraham et al. (1996) illustrate the power of photometric comparisons of galaxies across a range of environments to address the questions posed earlier. Both studies, however, only cover a single cluster and so it is not clear how general their conclusions are, especially given the cluster-to-cluster differences which could arise from different evolutionary histories.

This paper describes an analysis of the Las Campanas Observatory and Anglo–Australian Telescope Rich Cluster Survey (LARCS) to address this problem. LARCS is a long-term project to study a statistically-reliable sample of 21 of the most luminous X-ray clusters at intermediate redshifts ($z = 0.07$–0.16) in the southern hemisphere. We are mapping the photometric, spectroscopic and dynamical properties of galaxies in rich cluster environments at $z \sim 0.1$, tracing the variation in these properties from the high-density cluster cores out into the surrounding low-density field beyond the turn-around radius. For the most massive clusters at $z \sim 0.1$, the turn-around radius corresponds to roughly 1 degree or a 10 Mpc radius (O'Hely et al. 1998) and therefore we have obtained panoramic CCD imaging covering 2-degree diameter fields, as well as spectroscopic coverage of these fields (Pimbblet et al. 2001; O'Hely 2000; O'Hely et al. 1998). The imaging comes from B and R-band mosaics taken with the 1-m Swope telescope at Las Campanas Observatory, while the spectroscopy comes from the subsequent follow-up with the 400-fibre 2dF multi-object spectrograph on the 3.9-m Anglo-Australian Telescope (AAT).

The advantage of this sample for the present analysis is the homogeneity of the clusters and observations. This allows us to combine many clusters together to provide a large sample of cluster galaxies across a wide range in environment. In particular, we are able to use statistical corrections to remove field contamination, rather than requiring spectroscopic membership. We can thus investigate the colour of galaxies across a wide range in environments in clusters, spanning three orders of magnitude in projected galaxy density from the core out to close to the turn-around radius at ~ 8 Mpc.

In §2, we describe the LARCS cluster sample and the precision of our photometric catalogues. In §3 we outline the statistical method used to correct for field contamination and the construction of colour magnitude diagrams. In §4, we present our results on the characteristics of the galaxy populations in the clusters. By creating a composite cluster we explore the variation in the CMR with radius and local galaxy density. We discuss these results in §5 and present our conclusions in §6.

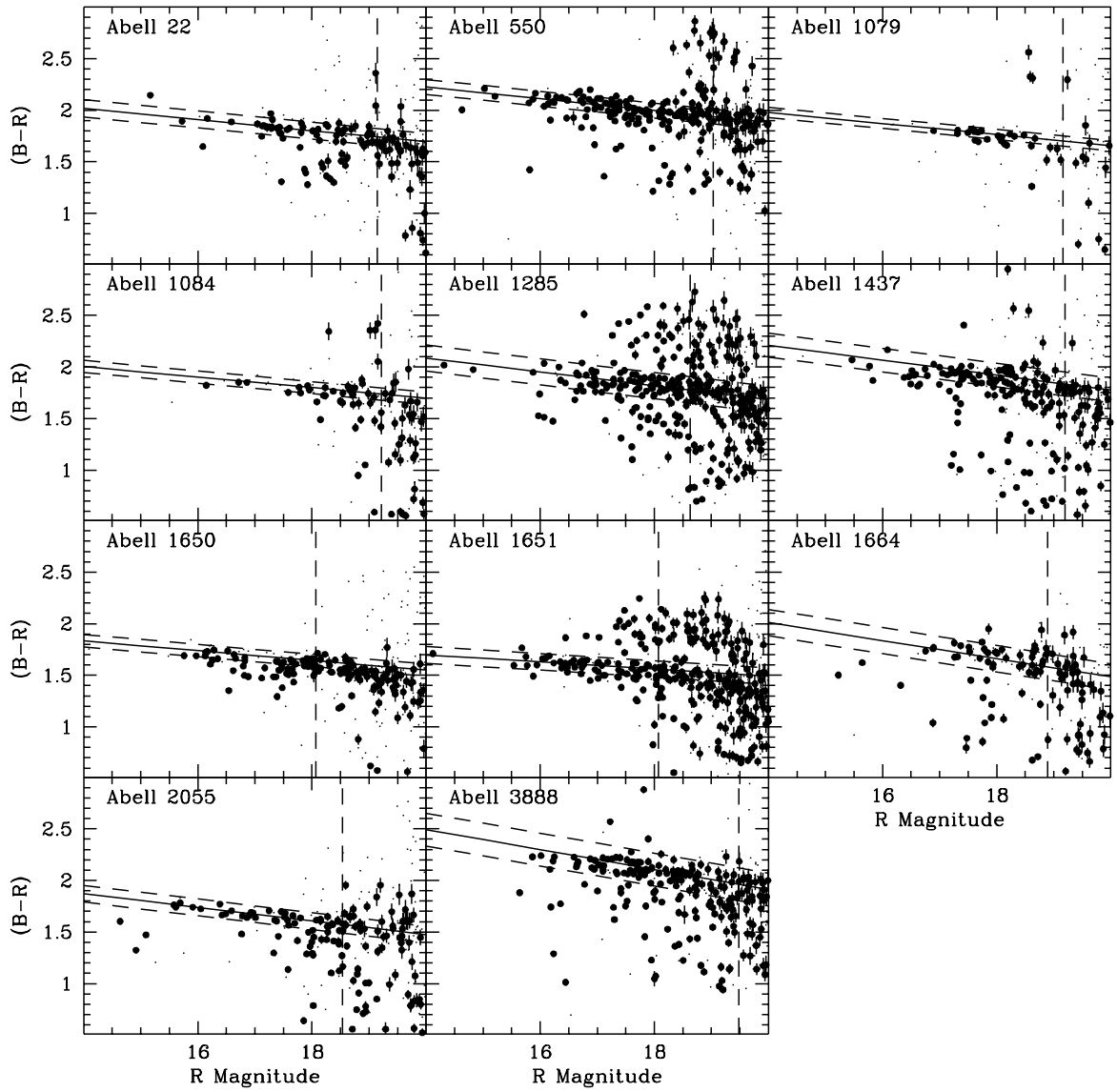

Figure 1. The colour-magnitude diagrams for the 11 clusters used in this work. All galaxies statistically-identified as cluster members within a 2 Mpc radius of the cluster centre from one realization of the field subtraction are plotted as heavy points. The smaller points are the galaxies which were rejected as field by our statistical subtraction method. The biweighted fit to the CMR is shown as a solid line. The 1σ uncertainty in the colour is shown by the flanking parallel dashed lines. The vertical line denotes the absolute magnitude limit of $M_V = -20$ used to define the galaxy sample used for the fit.

2 CLUSTER SELECTION AND OBSERVATIONS

The sample used in our analysis is from the LARCS survey (Pimbblet et al. 2001). LARCS is a survey of the properties of an X-ray luminosity-limited sample of 21 clusters at $z = 0.07$–0.16. The clusters in the sample are selected from the X-ray brightest Abell Clusters (XBACS) catalogue of Ebeling et al. (1996). XBACS comprises 242 Abell clusters detected in the *ROSAT* All-Sky Survey and is effectively a complete, volume-limited sample of the most X-ray luminous clusters, $L_X \gtrsim 5 \times 10^{44} \mathrm{erg\,s^{-1}}$, at $z \sim 0.1$. The 21 clusters in the LARCS sample are a random subsample of the southern XBACS clusters with $L_X > 3.7 \times 10^{44} \mathrm{erg\,s^{-1}}$ at $z = 0.07$–0.16.

Ten clusters from LARCS are analysed in this paper and we list them in Table 1 (an additional cluster, A 1079, is present in our observations of A 1084 and we have included it in our analysis). These ten clusters possess the highest quality and most complete photometric observations from the full survey. The subset covers a representative range of the complete LARCS sample, including clusters which ap-

pear relaxed in their X-ray and galaxy distributions (e.g. A 1650), as well as more dynamically young, disturbed looking systems (e.g. A 1664 – which appears to have undergone a recent cluster–cluster merger; Edge, priv. comm.).

High quality broad-band B- and R-band CCD images of each cluster have been obtained at Las Campanas Observatory using the 1-m Swope Telescope. More details of the observations, reduction and analysis of these data are given by Pimbblet et al. (2001); here we briefly summarise the pertinent points.

A 2°-diameter field around each cluster is imaged in 21 over-lapping pointings to produce a mosaic of a region out to ~ 10 Mpc radius at the survey's median redshift of $z \sim 0.12$. The images are reduced using standard tasks within IRAF and are then catalogued using the SExtractor package of Bertin & Arnouts (1995). We adopt "MAG_BEST" from SExtractor as the estimate of the total magnitudes. To determine colours for the sources we measure aperture photometry within 4″ diameter apertures (typically ~ 10 kpc at the cluster redshifts) on seeing-matched tiles using PHOT within IRAF. Photometric zeropoints are computed using frequent observations of standard stars (typically over 100 standard stars per broad-band filter per night) from Landolt (1992) interspersed throughout the science observations. On photometric nights, the variation in the resultant colour and extinction terms are all within 1σ of each other and the final photometric accuracy is better than 0.03 mags.

As some of the observations within a mosaic are undertaken in non-photometric conditions it is necessary to calibrate these independently. This is achieved through the method developed by Glazebrook et al. (1994). We use information on the photometry of objects in the overlapping regions of the tiles to calculate the offsets between photometric and non-photometric mosaic tiles. Once corrected by Glazebrook's algorithm, the resultant median tile-to-tile variation in zero-points across the mosaic is < 0.006 mags (see Figure 1 of Pimbblet et al. 2001), as estimated from the scatter in the magnitude from the duplicated sources in the overlapping regions. The maximum deviations between tiles is ~ 0.015 mags. We expect that the photometric zeropoint errors of 0.03 mags dominate the systematic error budget and the tile-to-tile variation in zero-points are small by comparison.

Finally, we apply corrections for galactic reddening based on Schlegel et al. (1998). The final internal magnitude errors across the full mosaics are typically 0.03 mag and always less than 0.06 mags (Pimbblet et al. 2001). Such accuracy is essential to detect subtle photometric radial gradients in the colour-magnitude relation. The catalogues are typically 80 percent complete at a depth of $R \sim 22.0$ and $B \sim 23.0$.

Star/galaxy separation for the catalogues uses the robust criteria described in Pimbblet et al. (2001): FWHM $>$ 2.0″ and CLASS_STAR < 0.1 from the SExtractor star–galaxy classifier. The resulting stellar contamination based on these criteria is estimated at ≤ 3 percent (see Pimbblet et al. 2001). To further check for misclassification of compact early-type cluster galaxies as stars we have constructed colour-magnitude diagrams for the star samples and confirm that they exhibit no hint of a CMR at the relevant colour for the cluster members.

3 CONSTRUCTION OF THE COLOUR-MAGNITUDE DIAGRAMS

In this section we describe the construction of colour-magnitude diagrams from the LARCS catalogues, the use of the biweight method to fit the CMR and the spatial distribution of the cluster galaxies (i.e. cluster morphology).

3.1 Statistical field correction

To examine the galaxy population of the clusters in the absence of spectroscopy it is necessary to correct for the "field" contamination in a given cluster catalogue. The statistical subtraction method utilized in this study is described in detail in Appendix A.

Briefly, the field population is determined from the outer regions of the LARCS cluster mosaics at a radius well beyond 6 Mpc (at a redshift of $z = 0.12$). The field regions from each cluster are all examined by eye prior to being stacked to give the average field distribution. After examining these data, we reject part of the field around Abell 1084 due to the presence of Abell 1079. The field sample is not significantly biased to a lower mean density because of its removal. Once generated, the final stacked field population† is then appropriately area-scaled to that of the cluster sample we wish to correct.

The colour-magnitude diagrams for galaxies from the cluster sample and the final, scaled, stacked field sample are then compared. By direct comparison of corresponding regions on the colour-magnitude diagrams we assign each galaxy in the cluster sample a probability of being a field galaxy. Then, using a Monte Carlo method, we subtract off the field population based upon these probabilities. As described in Appendix A, however, problems can arise if the calculated probability exceeds 1.0. The solution utilized in this work is to expand the interval in colour and magnitude used to calculate the probability until it lies in the range $0.0 < \mathrm{P(Field)} < 1.0$ (see Appendix A for a full discussion).

In this work, the statistical Monte Carlo background subtractions are realized 100 times and the colour-magnitude fits presented represent the median of those background subtractions.

3.2 Fitting the CMR

We run the background subtraction algorithm (see Appendix A) on each cluster to produce 100 realizations of the cluster's colour-magnitude diagram. In fitting the CMR we only use those galaxies whose absolute rest frame magnitude is brighter than $M_V = -20$. This magnitude is chosen to correspond to the equivalent limit in Butcher & Oemler (1984).

Each of the CMRs are fitted using a robust biweight method (Beers et al. 1990) identical to that employed by Terlevich (1998). Briefly, the biweight method is a statistically robust estimator that weights outlying points (such as the blue population) low in order to find the best fit

† The final effective area of our field sample is ~ 13.1 square degrees. Each cluster mosaic covers ~ 3.1 square degrees on the sky.

line to the CMR. In line with Beers et al. (1990), we adopt the median absolute deviation as the best estimator of the biweight location and scale and a value of the weighting parameter of $w = 6$, this results in zero-weight being given to galaxies more than 4σ away from the median relation with the weighting increasing quadratically closer to the median value (e.g. 95 per cent weighting at 1σ). Since we seek to fit a model to these data, we must minimize the residuals of the data to the model. Therefore the set of points $x_i = Y_i - f(X_i)$ are defined, where (X_i, Y_i) are the data points and $f(X)$ is the model (a straight line of the form $f(X) = mX + c$). The scale and location of the x_i are then iteratively minimized on the (m, c) plane using the multidimensional downhill simplex method of Press et al. (1992). We apply this routine to the background-subtracted cluster sample from each of the 100 Monte Carlo simulations. We adopt the median of the fit parameters from the 100 simulations as our best estimate of the CMR and use the scatter between the simulations to give the uncertainty in this fit. We note that our adoption of the errors from the Monte Carlo field correction may underestimate the uncertainty in the fits when the sample is dominated by the cluster population. Most of our analysis, however, lies in the regime where the field contribution is important and so we retain these errors as the best estimates of the internal uncertainty in our fits.

In Figure 1 we show the distribution of galaxies on colour-magnitude diagrams for one such realization of each of the clusters within a radial extent of $r_p < 2\,\mathrm{Mpc}$. Details of the median values of the fits to the 100 realisations for each cluster and their associated errors are presented in Table 1.

All the clusters show colour-magnitude relations for the redder, early-type galaxy members. We see strong CMRs (more than 60 galaxies lying on the CMR within 2 Mpc of the cluster centre) in A 550, A 1285 and A 3888; whilst A 1079, A 1084 and A 1664 exhibit much weaker relations (less than 25 galaxies lie on the CMR within 2 Mpc of the cluster centre). All the CMR's exhibit a negative slope as expected from the colour-luminosity relation of early-type galaxies (Table 1, Figure 2).

The colour at a fiducial magnitude of $M_V = -21.8$ (equivalent to an $L^\star$ galaxy) is also calculated from the result of the biweight fit; $(B-R)_{M_V=-21.8}$. These colours are presented in Figure 2 and tabulated along with the values of $M_V = -21.8$ in Table 1. The $(B-R)_{M_V=-21.8}$ colours of galaxies on the CMRs in the clusters form a tight relation, median deviation of 0.08 mags, which steadily reddens with redshift due to the K-correction. We also show the expected variation with redshift in the observed colour of a galaxy which formed all its stars at very high redshift, $z \gg 2$. The reddening in colour at the fiducial magnitude we see is broadly in line with that expected for a population which formed the bulk of its stars at high redshift (Metcalfe et al. 1991). The small scatter in the redshift trend implies that our cluster to cluster photometry is internally consistent.

The statistical field correction we apply is designed to detect overdensities above the level of the "average" field on the colour-magnitude plane. Therefore, if there are other over-dense regions in the fields of our clusters we expect to see some secondary CMRs in the colour-magnitude diagrams. Such CMRs are seen in the colour-magnitude diagrams of A 550, A 1285 and A 1651. As expected from the available volume, these CMRs are higher redshift clusters in the background of the observed clusters, for example, we identify the background cluster in A 1651 ($z = 0.084$) as A 1658 ($z \sim 0.145$). To reduce the influence of these systems on the biweight estimator used to fit the CMR of the LARCS cluster, we employ an appropriate red limit to ensure the fit converges on the desired CMR.

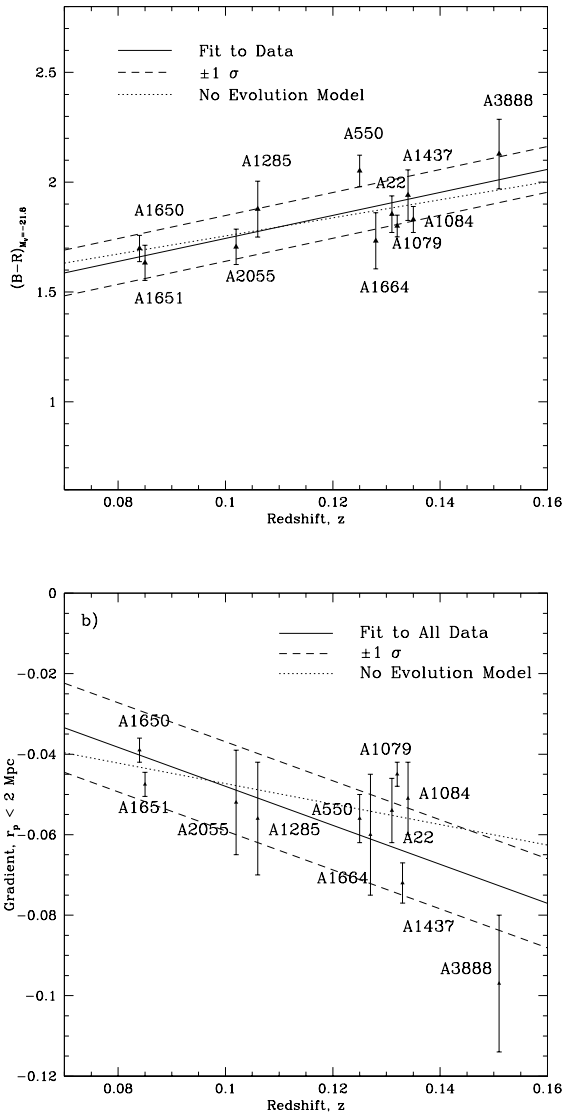

Figure 2. a) Median observed $(B-R)$ colour at $M_V = -21.8$ calculated from 100 realizations of the background subtraction plotted versus cluster redshift (with no K-correction applied). The solid line is the best fit to the data, with the parallel dashed lines being $\pm 1\sigma$. The dotted line illustrates the expected evolution in the galaxy colours of galaxies which formed all their stars at high redshift, $z \gg 2$. The clusters form a tight relation evolving redward with increasing redshift. **b)** The variation in slope of the CMR with redshift. There is a trend for steeper CMR's at higher redshifts, as expected from the effects of shifting K-corrections on the observed $(B-R)$ colours of the galaxies along the CMR. We show a "No evolution" model which shows the behaviour expected just from the differential K-corrections.

3.3 The spatial distribution of cluster galaxies

We now use the CMRs to map the two dimensional galaxy distribution within the clusters. Assuming that the galaxies on the CMR are associated with the cluster, we define a cluster galaxy to be within the 1σ scatter of its fitted colour-magnitude relation (listed in Table 1). This criteria is applied to the whole sample of galaxies in each field. Having obtained their positions on the sky, we use a circular top-hat function with a 500 kpc smoothing length to generate smoothed galaxy distribution maps for each cluster. The resultant distributions for the central $25'$ of each cluster are presented in Figure 3.

The brightest galaxy in these X-ray luminous clusters is typically a giant elliptical and we identify these using the CMR and the morphology of their extended low surface brightness halo in our imaging data. For the more regular clusters, the position of this galaxy is generally in agreement with the peak of the distribution of colour-selected cluster members (Figure 3) and we therefore use the position of this galaxy to define the cluster centre. Our clusters demonstrate a broad range of morphological types ranging from very regular, highly-concentrated examples (e.g. A 550), through to very diffuse systems (e.g. A 1664) whose central galaxy position does not coincide with any of the main spatial overdensities seen in the colour-selected cluster members.

4 ANALYSIS AND RESULTS

In this section we describe the analysis of the properties of the cluster's CMRs as a function of radius and local galaxy density.

4.1 Radial variation of the CMR

We search for any radial variations in the CMR within the clusters by dividing the central 6 Mpc diameter region of clusters into three anulii. We note that the virial radii for these X-ray luminous clusters should lie in the range 2–4 Mpc (Carlberg et al. 1996). For each radial bin, a biweighted fit is calculated to the CMR and the colour at a fiducial magnitude (equivalent to $M_V = -21.8$) is obtained. We have also calculated the colour based on a fixed slope (using the fit to the CMR in the central 2 Mpc diameter annulus) for the field-subtracted cluster realizations and found that this method produces the same results as an unconstrained gradient fit, within 1 standard deviation (see Table 2). The result of these fits are presented in Table 2, whilst the colour-magnitude relations for the three radial bins in each cluster can be seen in Figure 4.

In most of our clusters we observe a modest blueward shift in colour at the fiducial magnitude with radius by $\Delta(B-R) \sim -0.09 \pm 0.11$ out to 3 Mpc (Table 2). We see no significant change in this trend with cluster redshift. Discrepant results arise in three clusters. In A 1084, the change in $(B-R)$ colour from the central radial bin to the third is much more than $\Delta(B-R) \sim -0.10$. We attribute this to the poor fit in the third radial bin (see Figure 4). The third radial bin of A 3888 is similarly poorly fitted. In A 1664, no radial trend is apparent.

However, we note that there are two shortcomings of this analysis. Firstly, the formal errors on the biweighted fits for individual clusters are large enough that the colour gradient trend in the individual CMRs is insignificant. Secondly, the biases in the statistical correction of the colour-magnitude diagram make it increasingly unreliable at large radii (Appendix A). We must therefore adopt a different approach.

To trace the variation in the colour of the CMR out to larger radii and better quantify its strength, we can exploit the homogeneity of our cluster sample and observations by combining all of our clusters together into a single composite system. This will improve the statistics for cluster members at large radii and provide a more robust measurement of the trends in the CMR. In doing so, however, we acknowledge that there may be aperture bias present in our photometry: we use a fixed photometric aperture and therefore cluster galaxies will be sampled to different physical radii as a function of redshift. This effect may alter our determined CMR slopes and colour changes if there are strong colour gradients present within our cluster galaxies. We estimate that at least 85 per cent of the total light falls into our large $4''$ apertures (~ 10 kpc at $z \sim 0.12$; see §2) in all but the largest of our galaxies. As the nature of this work is a differential radial analysis of the composite CMR, we consider such an effect to be small.

To produce a composite cluster we have to transform the magnitudes, colours and positions of the galaxies in the individual clusters onto a common scale. The transformation of the magnitudes uses the relative magnitudes of non-evolving early-type $L^\star$ galaxies from Table 1, an assumption which is supported by the agreement between the no evolution predictions for colour evolution and the observations across the limited redshift range spanned by our sample. The apparent magnitudes of the galaxies can therefore be transformed to a median redshift of $z = 0.12$. To transform the colours of the galaxies on the CMR onto a uniform scale we simply reduce the observed CMR's to provide colours relative to the fitted relation. These can then be easily transformed to $z = 0.12$. The slope we adopt for this transformation is assumed to be constant with radius, and equivalent to the measured values presented in Table 1. We emphasize that our slopes are determined in a totally homogeneous manner for a homogeneous sample: two absolute requirements given the uncertainties. The most meaningful method to compare the radial positions of galaxies in the various clusters is to use their radius normalised to the virial radius of the clusters, $R_{\rm vir}$. However, the weak dependence of the virial radius on the X-ray luminosity, $R_{\rm vir} \propto L^{1/6}$ (Babul et al. 2001), combined with a narrow X-ray luminosity range for our sample, means that $R_{\rm vir}$ is only expected to vary by 20 percent across the whole sample. Hence, for simplicity, the clusters are all scaled to a fixed metric size.

The final step in our analysis of the composite cluster is to construct colour histograms down to the fiducial magnitude limit, $M_V = -20$. These histograms are statistically corrected using the binned colour distribution from the field. We can use this approach as we are interested in the typical colour of the CMR, rather than its slope, so we no longer need to retain the magnitude information on the galaxies. The advantage of using colour histograms is that it circumvents some of the concerns about the field correction techniques used on the colour-magnitude plane (Appendix A).

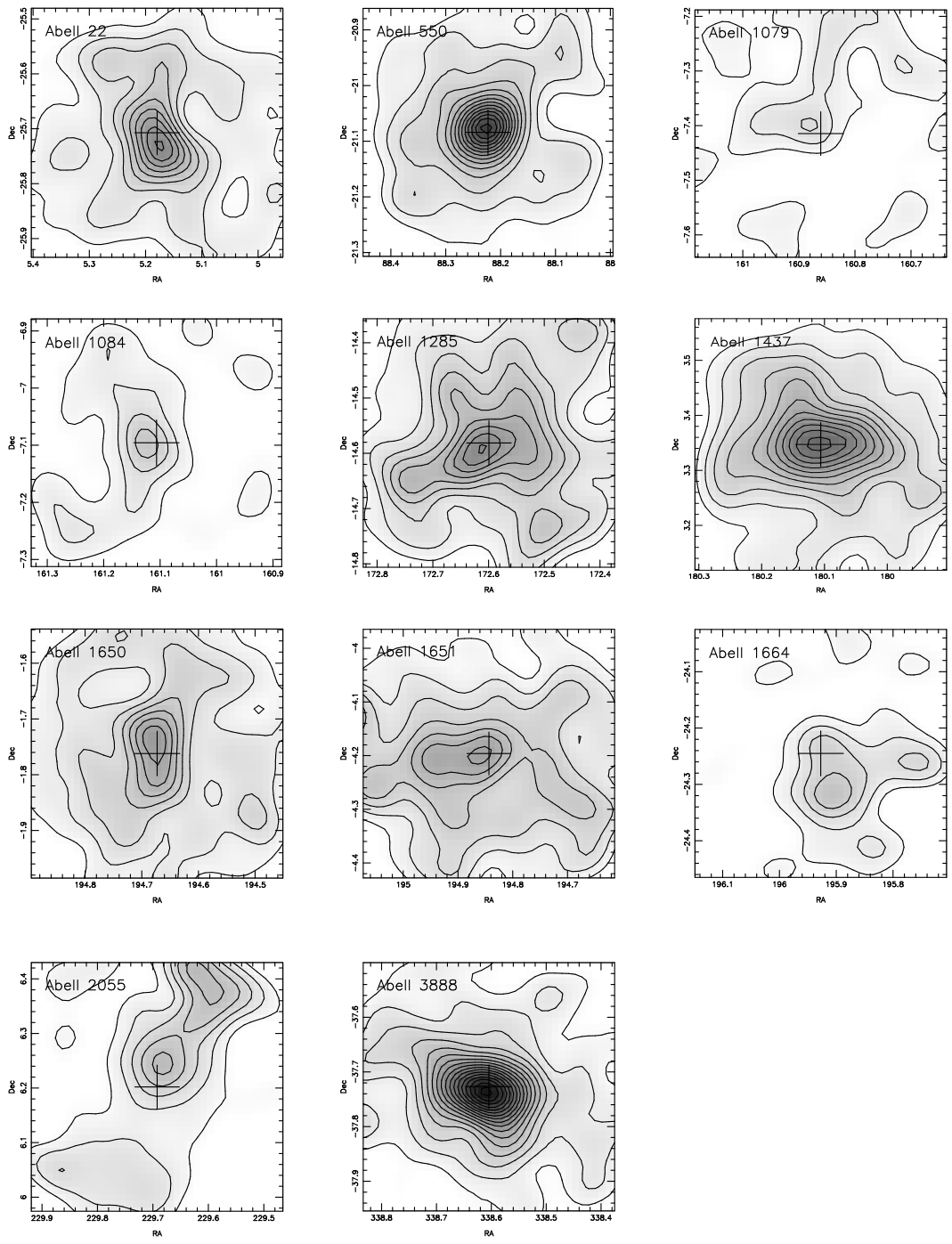

Figure 3. The two dimensional smoothed spatial distributions of the cluster galaxies lying within the scatter of the biweight fit to the CMR. A circular top-hat function with a 500 kpc smoothing length is used on the positions of galaxies to generate these maps. The lowest contour represents a surface density of cluster galaxies of $6.0\,\mathrm{Mpc}^{-2}$, with each subsequent inward contour denoting an increase of $2.0\,\mathrm{Mpc}^{-2}$. The crosses indicate the adopted centre of the clusters based on the position of the apparent brightest cluster member from the CMR.

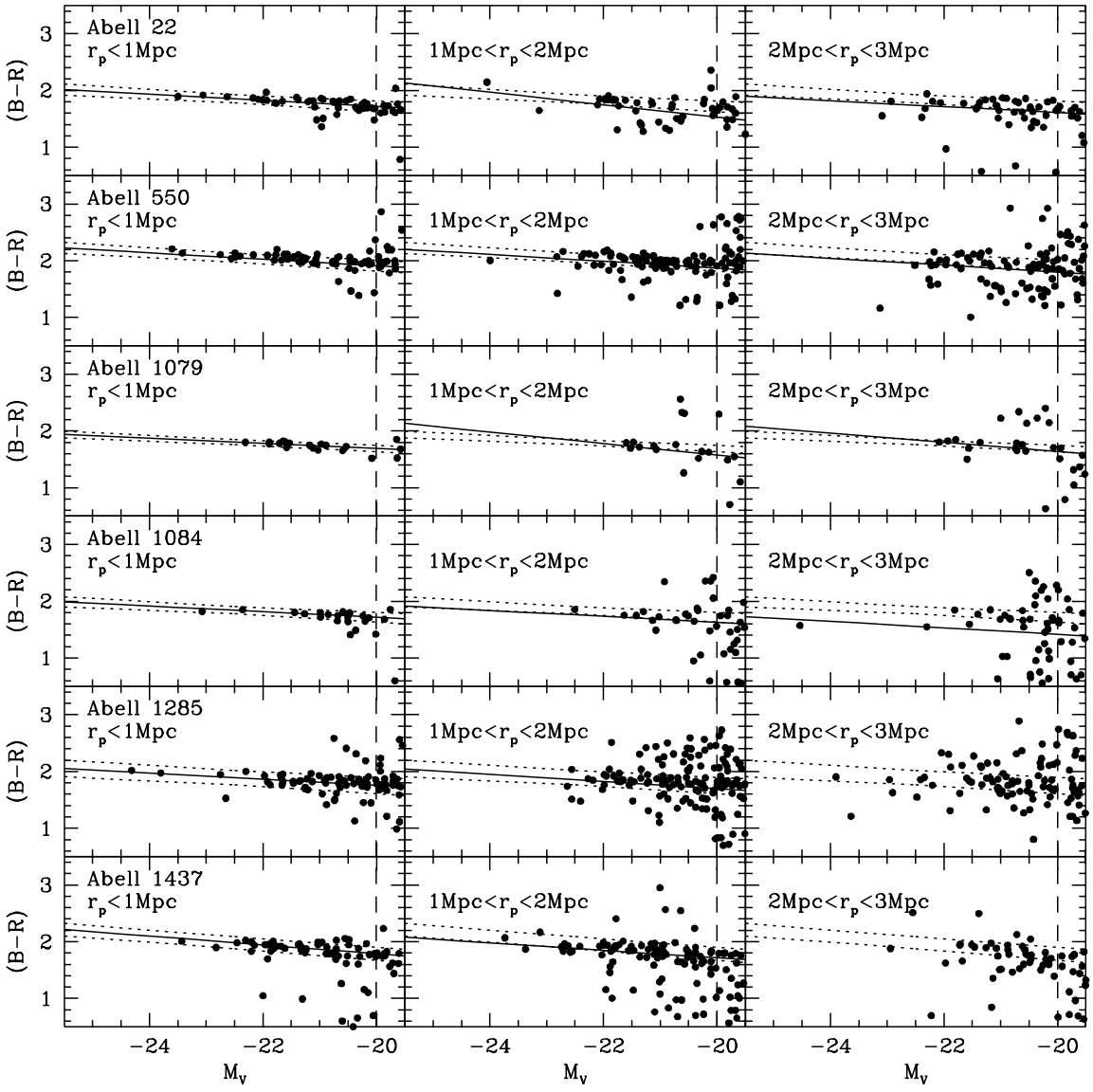

Figure 4. (a) Colour-magnitude diagrams for A 22, A 550, A 1079, A 1084, A 1285 and A 1437 in 1-Mpc wide radial bins. Each diagram shows one of the 100 realizations made with the background subtraction algorithm. The solid line, where present, is the biweighted fit to the CMR; if absent, a biweighted fit could not be successfully made. The short dashed lines denote the combined errors associated with the $r_p < 1\,$Mpc fit of each cluster. The longer dashed, vertical lines denote the $M_V = -20$ fiducial magnitude limit; only galaxies brighter than this are considered in the biweighted fit. For most of the clusters, there is a trend for the CMR to evolve bluewards by $\Delta(B-R) \sim -0.09 \pm 0.11$ out to 3 Mpc.

We create the colour histogram of the field sample in an identical manner to the cluster sample. An appropriately area-scaled region of the field is subtracted off the composite cluster histogram in each radial bin. The result of this analysis is illustrated in Figure 5.

Figure 5 shows that the red cluster members in the CMR are still visible as a peak in the colour histogram as far out as $\sim 6\,$Mpc from the cluster core. Beyond this, the red galaxies become swamped by an increasingly blue cluster population and the noise from the statistical field correction. To identify the peak in the CMR and quantify how it changes with radius we fit the colour histograms with a gaussian using a χ^2 minimization method. To make the fit we restrict the colour range to $(B-R) = 1.6$–2.2. An initial estimate of the modal colour, its amplitude and the width of the distribution, σ_{PEAK}, is made and fed in as the input to the gaussian fitting routine. The routine outputs new estimates of these values which are iteratively returned to the fitting routine until convergence is achieved. The resultant values are checked by visually inspecting the fit. The

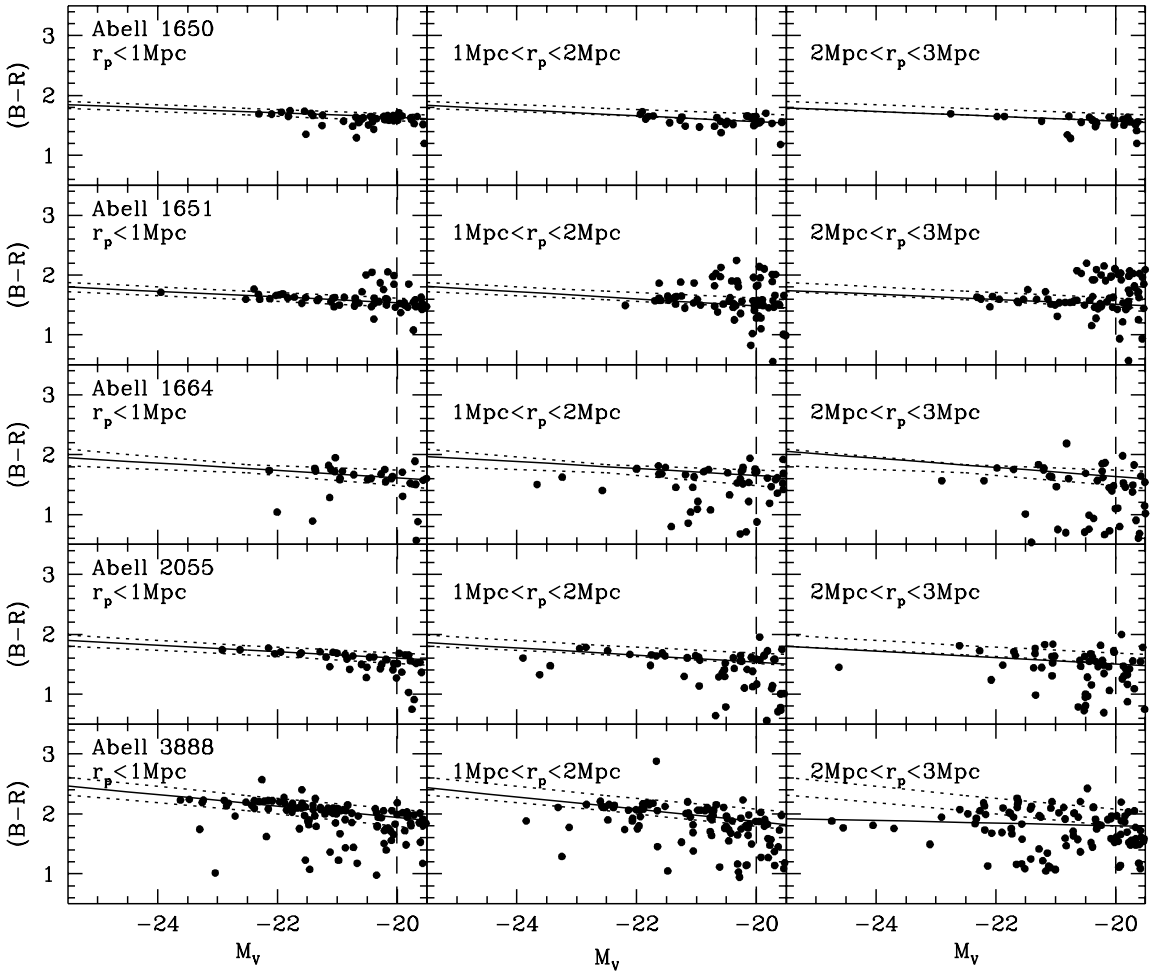

Figure 4. (b) As for Figure 4a, but with A 1650, A 1651, A 1664, A 2055 and A 3888.

gaussian fits generate the colour of the CMR at the fiducial magnitude and a measure of the width of the CMR, together with associated errors, in each radial interval. The fits are presented in Table 3 and illustrated in Figure 5. The peak of the CMR in the combined cluster evolves bluewards with radius at a rate of $d(B-R)/dr_p = -0.022 \pm 0.004$ (where r_p is the projected radius from the cluster core), equivalent to $\Delta(B-R) \sim -0.11 \pm 0.05$ from the central radial bin out to 6 Mpc. Beyond 6 Mpc the constraints on the colour gradient trend of the CMR become less reliable and so we limit our discussion to the region within 6 Mpc.

4.2 The colour–local density relation

As the clusters in our survey exhibit a wide range in their morphologies (see Figure 3), we seek a more general method of combining the galaxy samples from the different clusters, rather than simple radial-averaging, to investigate the environmental differences within the composite sample. Local galaxy density provides a comparable measure of environment across the sample and so we employ this instead.

We calculate the local projected density for each galaxy in our clusters and use it to assign the galaxy to its relevant environmental bin. The local galaxy density, Σ, is estimated by finding the surface area on the sky occupied by that galaxy and its ten closest neighbours down to the fiducial magnitude limit of $M_V = -20$. Due to field galaxy contamination, this local density will be over-estimated. We correct for this by subtracting off a constant density estimated from the median local density of our combined field sample. We divide our sample up into eight logarithmically-spaced bins covering three orders of magnitude in local galaxy density (Table 3).

For each local density bin a colour histogram is created. As before, the clusters are transformed to a median redshift of $z = 0.12$ and the slope of the CMR is corrected for. Since these colour histograms are not corrected for field contamination, it is necessary to subtract off an appropriately area-scaled colour distribution for our field sample (see the lower-right panel in Figure 5). Finding the area from which a restricted range of densities are drawn is non-trivial; a region of high density will have a much smaller field correction

Table 2. Parameters of the biweight fit to the CMRs of the clusters, split into three equal radial bins as plotted in Figure 4. The slope and colours are those found using the biweight estimator fit to each radial bin. The values reported in the final column (fixed slope) uses the slope of the central bin in the particular cluster. The errors are the 1σ variation from the 100 Monte Carlo simulations of the background subtraction.

Cluster	Radius (Mpc)	Slope	$(B-R)_{M_V=-21.8}$	$(B-R)_{M_V=-21.8}$ Fixed Slope
A 22	0–1	-0.054 ± 0.008	1.85 ± 0.07	1.85 ± 0.07
	1–2	-0.110 ± 0.010	1.87 ± 0.12	1.73 ± 0.21
	2–3	-0.052 ± 0.007	1.75 ± 0.17	1.73 ± 0.22
A 550	0–1	-0.057 ± 0.001	2.05 ± 0.07	2.05 ± 0.07
	1–2	-0.060 ± 0.003	2.02 ± 0.15	2.02 ± 0.14
	2–3	-0.061 ± 0.014	1.94 ± 0.35	1.92 ± 0.38
A 1079	0–1	-0.045 ± 0.003	1.80 ± 0.05	1.80 ± 0.05
	1–2	-0.101 ± 0.004	1.82 ± 0.07	1.76 ± 0.09
	2–3	-0.081 ± 0.009	1.82 ± 0.20	1.85 ± 0.33
A 1084	0–1	-0.050 ± 0.009	1.83 ± 0.06	1.83 ± 0.06
	1–2	-0.052 ± 0.014	1.78 ± 0.42	1.79 ± 0.31
	2–3	-0.057 ± 0.027	1.55 ± 0.54	1.66 ± 0.56
A 1285	0–1	-0.055 ± 0.007	1.87 ± 0.12	1.87 ± 0.14
	1–2	-0.060 ± 0.013	1.86 ± 0.33	1.86 ± 0.34
	2–3	...	...	...
A 1437	0–1	-0.077 ± 0.005	1.94 ± 0.10	1.94 ± 0.12
	1–2	-0.065 ± 0.003	1.87 ± 0.21	1.87 ± 0.21
	2–3	...	...	...
A 1650	0–1	-0.038 ± 0.001	1.70 ± 0.06	1.70 ± 0.06
	1–2	-0.050 ± 0.005	1.65 ± 0.08	1.65 ± 0.08
	2–3	-0.041 ± 0.011	1.63 ± 0.07	1.65 ± 0.06
A 1651	0–1	-0.047 ± 0.002	1.63 ± 0.07	1.63 ± 0.08
	1–2	-0.060 ± 0.011	1.63 ± 0.16	1.64 ± 0.24
	2–3	-0.048 ± 0.008	1.59 ± 0.15	1.60 ± 0.14
A 1664	0–1	-0.062 ± 0.012	1.73 ± 0.07	1.73 ± 0.07
	1–2	-0.058 ± 0.039	1.76 ± 0.07	1.76 ± 0.08
	2–3	-0.076 ± 0.024	1.76 ± 0.08	1.76 ± 0.08
A 2055	0–1	-0.054 ± 0.007	1.71 ± 0.08	1.71 ± 0.08
	1–2	-0.050 ± 0.021	1.67 ± 0.15	1.62 ± 0.18
	2–3	-0.054 ± 0.024	1.67 ± 0.26	1.60 ± 0.28
A 3888	0–1	-0.096 ± 0.015	2.13 ± 0.13	2.12 ± 0.13
	1–2	-0.103 ± 0.043	2.08 ± 0.22	2.04 ± 0.25
	2–3	-0.193 ± 0.013	1.88 ± 0.35	1.90 ± 0.36

than a region of low density. We generate an adaptive map of the field region by binning up the positions of the field galaxies and taking the median density of each bin. The map is thresholded using density cuts equal to the eight logarithmically-spaced bins in local galaxy density to generate the area occupied by galaxies of that local galaxy density. This measure of the area is used to scale the colour distribution of the field sample and subtract it from each local density bin's colour histogram.

The results of this analysis are presented in Figure 6. Our combined cluster evolves bluewards with decreasing local density at a rate of $d(B-R)/d\log_{10}(\Sigma) = -0.076 \pm 0.009$, equivalent to $\Delta(B-R) \sim -0.20 \pm 0.06$ from the highest local density regime covered by our sample ($\log_{10}(\Sigma) > 2.5$) to three orders of magnitude lower. The results from this analysis provide a comparable estimate of the shift in the CMR colour to that identified in §4.1 (for the typical cluster in our sample a local galaxy density of $\log_{10}(\Sigma) \sim 0.5$ corresponds to a radius of $\sim 2\,$Mpc).

4.3 Width of the CMR

From the histograms presented in Figures 5 and 6, we now examine how the width of the CMR varies with environment. The gaussians fitted to these data in the figures are used to obtain $\sigma_{\rm Peak}$ which we use as an estimate of the CMR's width. These values are plotted in the upper panels of Figure 7, with tabulated values presented in Table 3. We find that the CMR peak does appear to broaden with increasing radius and decreasing local galaxy density by $\Delta\sigma_{\rm Peak}(B-R) \sim 0.15$ across the ranges studied, although there is considerable uncertainty in the individual measurements.

To further investigate how the colour distribution of galaxies in the CMR varies with environment we also cal-

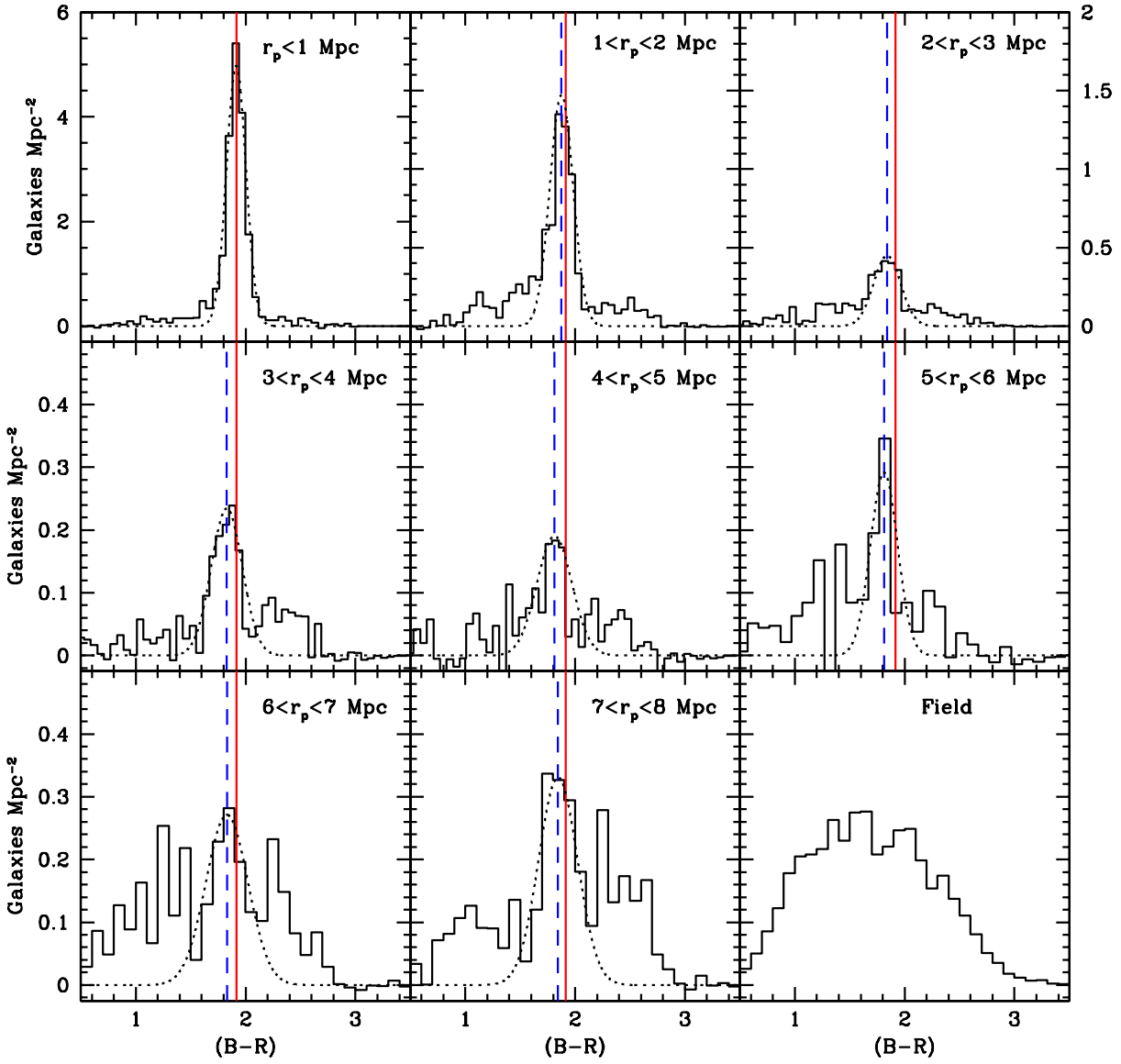

Figure 5. Colour histograms of the composite cluster from the center to a maximum radial extent of 8 Mpc. The field colour distribution is also pictured in the lower-right for reference (arbitrarily scaled). The best fit gaussians are shown for the CMR peaks in each radial bin. The solid vertical line is the colour of the CMR peak in the central bin. The dashed vertical line is the peak of each individual radial bin. A blueward shift in the peak of the CMR can be seen clearly even by the second radial interval, although the position of the CMR peak becomes more uncertain at large radii. The CMR evolves blueward at a rate of $d(B-R)/dr_p = -0.022 \pm 0.004$ from the centre to the outer regions. Also note that the CMR appears to the broaden at larger radius.

culate the colours of the 30$^{\rm th}$ and 70$^{\rm th}$ percentiles from the red end of the colour distributions (Figures 5 & 6). The 30$^{\rm th}$ percentile represents the reddest members of the CMR peak, the typical colour of this population appears to remain nearly constant in colour (Figure 7) out to ~ 6 Mpc (i.e. the limit of the visibility of the CMR in Figure 5). Beyond 6 Mpc, there is a reddening of this colour which we believe is due to CMRs of other higher redshift clusters. A similarly selected sample exhibits the same near constant trend in colour with local galaxy density. In contrast, the trend of the 70$^{\rm th}$ percentile, representing the bluer members of the CMR, shows a strong shift to the blue with both radius and local galaxy density.

Thus whilst the colour of the reddest members of the CMR appears to be relatively constant in different environments, the width of the CMR peak broadens at larger radii and lower local galaxy density, reflecting an increasing tail of blue galaxies on the outskirts of the clusters (see Figures 5, 6 & 7).

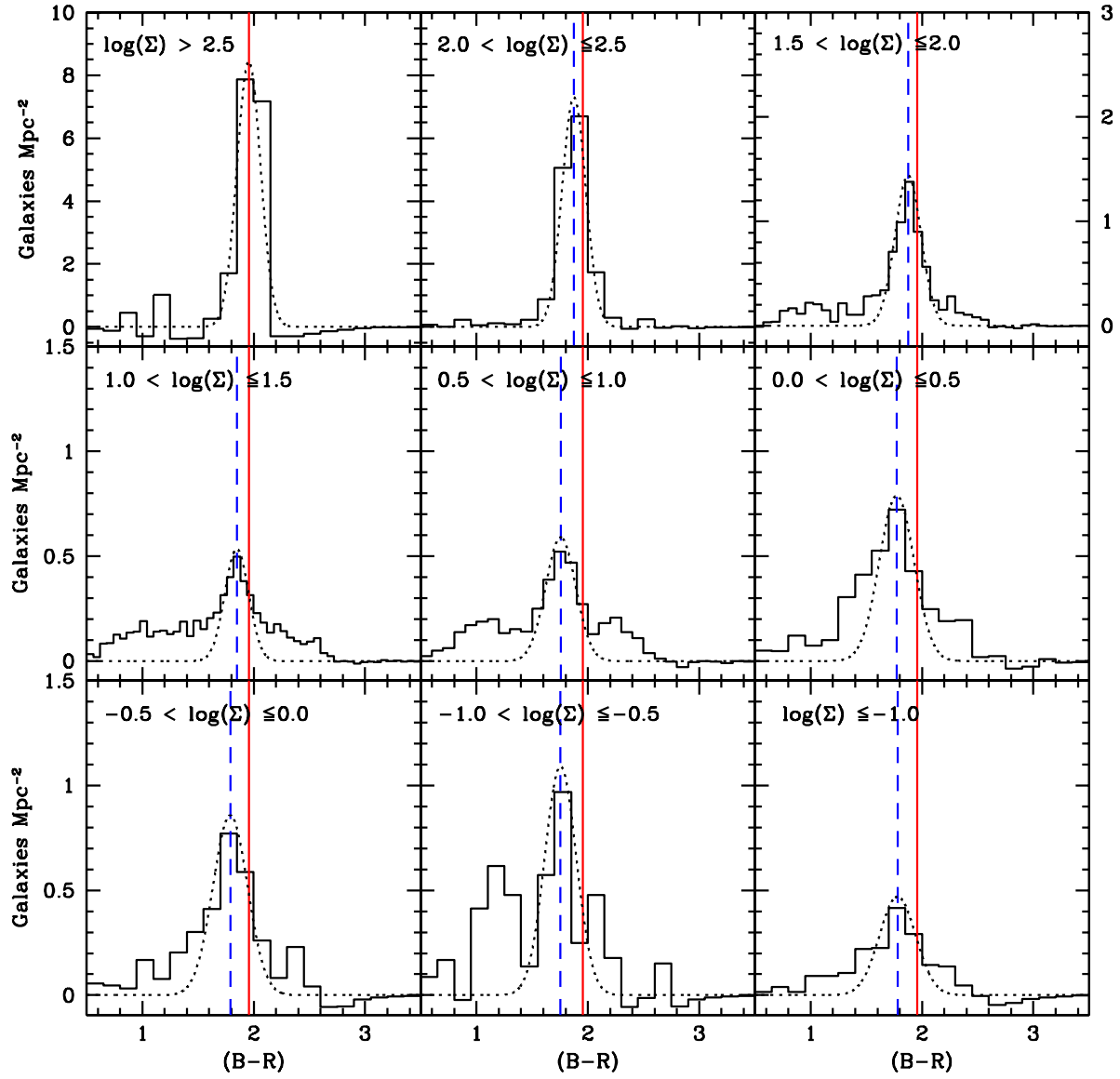

Figure 6. Colour histograms of the composite cluster colour magnitude relations in logarithmic density intervals after correcting for the slope in the CMR and field contamination. The best-fit gaussians are shown for the CMR peaks in each density bin. The solid vertical line shows the colour of the peak of the CMR in the highest density bin. The dashed vertical line is the peak in the particular density interval. The CMR peak evolves steadily blueward at a rate of $d(B-R)/d\log_{10}(\Sigma) = -0.076 \pm 0.009$ across three orders of magnitude in local galaxy density (Σ).

4.4 Blue cluster galaxies

We now compare the relative proportions of the red and blue galaxies in the clusters. To do this we quantify the fraction of non-CMR galaxies by deriving the Butcher-Oemler blue fraction (Butcher & Oemler, 1984), f_B. The blue fraction is calculated for all of our clusters using the method described in Butcher & Oemler's (1984) landmark study. Briefly, to calculate f_B we use only those galaxies whose magnitude is brighter than $M_V = -20$ and lie within a radius of R_{30}: the radius of a circle containing 30 percent of the cluster's projected galaxy distribution. After background subtraction, the net number of galaxies in these populations are a measure of cluster richness, denoted N_{30}. The blue fraction is the fraction of this population whose rest frame colour is $\Delta(B-V) = -0.2$ bluer than the fitted CMR. The concentration of the cluster is defined as $\log_{10}(R_{60}/R_{20})^{\ddagger}$ and is

‡ The radius R_α is the radius of a circle containing α per cent of the cluster's projected galaxy distribution.

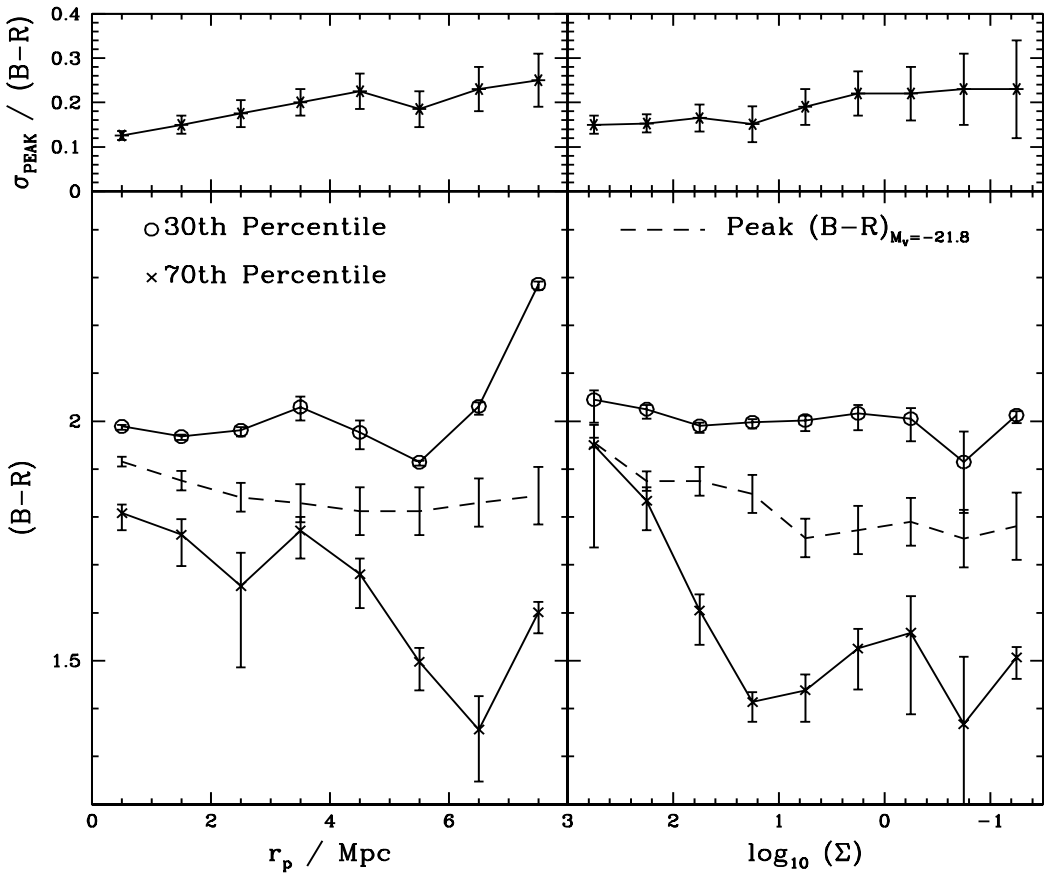

Figure 7. The 30$^{\rm th}$ and 70$^{\rm th}$ percentiles of the colour histograms presented in Figures 5 & 6, measured relative to the red end of the distribution. These are plotted in the two lower panels as a function of radius and local galaxy density (solid lines) together with the peak CMR colour (dashed line) taken from Figure 5. The 30$^{\rm th}$ percentile of the distributions is near constant over at least the inner 6 Mpc of our combined cluster whilst the peak shifts to the blue by -0.11 ± 0.05 mag. We suggest that the sharp redward trend seen at large radii may result from the presence of background clusters and groups which dominate the red wing at the largest radii. The upper panel displays the width of the gaussian, $\sigma_{\rm Peak}$, fit to the colour histograms against radius. The width steadily increases by ~ 0.15 mag across the radial range. Similar behaviour is seen in the distributions when sorted in terms of local galaxy density.

a measure of the cluster's central concentration (Butcher & Oemler 1978, 1984).

We present in Table 4 the median value of f_B for the clusters and the associated values of R_{30}, N_{30} and the concentration. Also noted are the morphologies of the clusters from Figure 3.

We stress that these values of f_B are likely to be slightly low due to the biases in the statistical background correction technique employed. See Appendix A for discussion on this point. There may also be biases arising from the field sample we use. Since they are taken at the very edge of the cluster they may be fractionally more dense than the 'average' field thus further underestimating f_B. We consider this effect to be small and the statistical background correction to be the dominant source of any bias.

There is considerable scatter in the value of f_B in the clusters in our sample. In the majority of our clusters the blue fraction is negligible and, combined with the small range in X-ray luminosity and redshift covered by our sample, it is difficult to distinguish any trends in these parameters. There are two clusters, however, which do have significant blue populations: A 1437 and A 3888. Both of these clusters show evidence for recent merger events (Edge, priv. comm.) and appear highly concentrated in X-ray. The large scatter in f_B for the clusters in our homogeneous sample is surprising and suggests that this parameter is sensitive to short term events which affect the galaxy mix within the clusters.

5 DISCUSSION

We have examined variation of the CMR with environment; both with radius and with local galaxy density. We find that

Table 3. Peak colour and full width of the CMR's variation with radius and local galaxy density as estimated from the fitting gaussians to the colour distributions (Figures 5 & 6).

Sample	Peak $(B-R)_{M_V=-21.8}$	$\sigma_{\rm Peak}$
Radius (Mpc)		
0–1	1.92 ± 0.01	0.13 ± 0.01
1–2	1.88 ± 0.02	0.15 ± 0.02
2–3	1.84 ± 0.03	0.18 ± 0.03
3–4	1.83 ± 0.04	0.20 ± 0.03
4–5	1.81 ± 0.05	0.23 ± 0.04
5–6	1.81 ± 0.05	0.19 ± 0.04
6–7	1.83 ± 0.05	0.23 ± 0.05
7–8	1.84 ± 0.06	0.25 ± 0.06
Log Density (Mpc^{-2})		
> 2.5	1.96 ± 0.01	0.15 ± 0.02
2.0–2.5	1.88 ± 0.02	0.15 ± 0.02
1.5–2.0	1.87 ± 0.03	0.17 ± 0.03
1.0–1.5	1.85 ± 0.04	0.15 ± 0.04
0.5–1.0	1.76 ± 0.04	0.19 ± 0.04
0.0–0.5	1.77 ± 0.05	0.22 ± 0.05
−0.5–0.0	1.79 ± 0.05	0.22 ± 0.06
−1.0– −0.5	1.76 ± 0.06	0.23 ± 0.08
< -1.0	1.78 ± 0.07	0.23 ± 0.11

Table 4. Median values for the Butcher-Oemler blue fraction, f_B, taken from 100 realizations of the statistical background subtraction. The errors on f_B are one standard deviation from the median. Values of R_{30}, N_{30} and the concentration, Conc, (Butcher & Oemler 1979) derived from the calculation of f_B are also tabulated. The cluster's two-dimensional distribution of CMR members is also qualitatively described: Regular, R; Irregular, I.

Cluster	f_B	R_{30} (Mpc)	N_{30}	Conc	Morph.
A 22	0.02±0.02	1.06	44	0.29	R
A 550	0.04±0.01	1.35	96	0.32	R
A 1079	0.00±0.05	1.32	20	0.24	I
A 1084	0.05±0.03	1.78	37	0.27	I
A 1285	0.03±0.01	1.40	92	0.30	R
A 1437	0.19±0.02	1.11	47	0.33	R
A 1650	0.00±0.04	0.52	27	0.31	R
A 1651	0.00±0.02	1.19	50	0.29	R
A 1664	0.07±0.03	1.20	29	0.28	I
A 2055	0.06±0.03	1.26	36	0.29	R
A 3888	0.21±0.02	1.01	63	0.36	R

the CMR peak evolves bluewards and broadens with both radius and local galaxy density (Figures 5, 6 & 7). Yet the colour of the reddest members of the CMR remains constant (Figure 7). We emphasize at the outset of our discussion that the effects of environment upon galaxy evolution (e.g. star formation suppression, triggering and the morphological evolution of galaxies) are still polemical issues in modern astronomy (Dressler et al. 1997; Lubin et al. 1998; Andreon 1998; van Dokkum et al. 1998). In this section, we examine possible causes for these effects with particular reference to the S0 evolution proposed by the MORPHS team (e.g. Dressler et al. 1997; Poggianti et al. 1999).

5.1 The effects of morphology on the CMR

We now estimate the trends which should exist in our sample due to the existance of a morphology-radius relation (T–R, Whitmore & Gilmore 1991; Whitmore et al. 1993) or a morphology-density relation (T–Σ, Dressler 1980). We adopt a null hypothesis that the colour gradient we observe in the CMR with environment is due to an increasing fraction of early-type spiral galaxies in the cluster sample, while the colours of the spheroidal galaxies (ellipticals and S0s) are unaffected by their environment. This hypothesis is suggested by the fact that we see a broadening of the colour-magnitude relation with radius, but a fixed red envelope (Figure 7).

Although we really do not have detailed morphological classifications for our sample, we can use the distribution of galaxies in terms of concentration index (CI) and peak surface brightness ($\mu_{\rm MAX}$) to look for changes in the morphological mix in different environments within the clusters. On the CI–$\mu_{\rm MAX}$ plane, early-type galaxies populate the high-concentration and high surface brightness region, with later-types typically having lower concentrations and fainter peak surface brightnesses (Abraham et al. 1994; Pimbblet et al. 2001). Comparing the distribution in CI–$\mu_{\rm MAX}$ of galaxies lying on the CMR in the cluster core ($r_p < 1$ Mpc) and outskirts ($r_p > 4$–6 Mpc) we also find evidence for a shift in the typical morphology – with the outer regions having a larger proportion of lower-concentration, lower-surface brightness galaxies than the core. To quantify this difference, we use a two dimensional Kolmogorov-Smirnov (K-S) test (Fasano & Franceschini 1987) to show that the CI–$\mu_{\rm MAX}$ distribution for the $r_p < 1$ Mpc and $r_p > 4$–6 Mpc samples are unlikely to be drawn from the same parent population at 97.5 per cent confidence. Unfortunately, it is non-trivial to transform the observed shift in the CI–$\mu_{\rm MAX}$ distribution between these environments into expected colour differences.

There is another approach we can use to test our null hypothesis: we can evaluate the typical $(B-R)$ colour of the galaxy distribution in the clusters based on Whitmore & Gilmore's (1991) radial morphological mix and Dressler's (1980) local-density morphological mix. We adopt the morphological mix in local rich clusters on the assumption that it is unlikely to change dramatically from $z = 0$ to $z = 0.12$ (Fasano et al. 2001; Dressler et al. 1997). Our limiting magnitude of $M_V = -20$ is also broadly comparable with Dressler's (1980) limit of $M_V \sim -20.4$. We use the $(B-V)$ colours of the different morphological types from the Third Reference Catalogue (RC3, de Vaucouleurs et al. 1991) as illustrated in Roberts & Haynes (1994) and assume a no-evolution K-correction based on the SEDs in King & Ellis (1985). We split the sample into broad morphological types corresponding to those employed by Dressler (1980) and Whitmore & Gilmore (1991): E, S0 and S+Irr. The $(B-V)$ colours of E and S0 galaxies from the RC3 are $(B-V) = 0.90$ and 0.89 respectively. These correspond to observed $(B-R)$ colours at $z = 0.12$ of $(B-R) = 1.94$ for E's and $(B-R) = 1.91$ for S0s. The third morphological class is "S+Irr": comprising spiral and irregular galaxies. The use of this class in our analysis, however, is problematic due to its broadness. The CMR will not contain many of the later-type spirals (e.g. Sc and Sd) as their mean colours lie significantly bluewards of the CMR defined by elliptical and S0 galaxies.

Table 5. Relative changes in the colours of the cluster population at $z = 0.12$, compared to the galaxy population in the cluster core, assuming the morphological mixes from Whitmore & Gilmore (1991) and Dressler (1980). A blueward shift of -0.07 mags in $(B-R)$ is predicted from the centre out to 4 Mpc and -0.08 mags over a two orders of magnitude change in local density from the core.

Sample	E	S0	Sa/Sab	$\Delta(B-R)_{M_V=-21.8}$
Radius (Mpc)				
0–1	0.27	0.67	0.06	0.00
1–2	0.25	0.60	0.15	−0.04
2–3	0.23	0.59	0.18	−0.05
3–4	0.21	0.56	0.23	−0.07
Log Density (Mpc^{-2})				
>2.5	0.45	0.55	0.00	0.00
2.0–2.5	0.43	0.53	0.04	−0.02
1.5–2.0	0.36	0.55	0.09	−0.04
1.0–1.5	0.29	0.56	0.15	−0.07
0.5–1.0	0.21	0.59	0.20	−0.09
0.0–0.5	0.20	0.57	0.23	−0.10

To examine which morphological types from the "S+Irr" class are likely to inhabit the CMR we estimate how blue a galaxy has to be before it falls outside of the CMR peak and hence does not affect our gaussian fitting to the colour distributions (Figures 5 & 6). We estimate that galaxies as blue as $(B-R) \sim 1.5$–1.6 will affect the fitting of the CMR in the outskirts of the clusters; this corresponds to $(B-V) \sim 0.7$ at $z = 0$ or the colour of an Sab galaxy from RC3. At $z = 0.12$, an Sa galaxy will have a mean colour of $(B-R) = 1.55$ while Sab's have $(B-R) = 1.49$. Hence, we expect that it is only the Sa/Sab class from the spiral population which is likely to influence the colour of the CMR based on our fitting procedure. We therefore use Sa/Sab as our third morphological class, instead of the broader "S+Irr" class. Before we calculate the expected colour of the CMR peak we re-normalize the T–R and T–Σ morphological mixtures to account for using only Sa/Sab galaxies. This again is done using the RC3, from which we estimate the fraction of Sa/Sab galaxies within the "S+Irr" class and then re-scale the relative proportions of the three morphological classes (Table 5).

The gradient in mean $(B-R)$ colour predicted from the variation in morphological mix seen in the T–R relation (Table 5) is $d(B-R)/dr_p = -0.017$. This is equivalent to a change of $\Delta(B-R) = -0.07$ out to 4 Mpc which is roughly 75 percent of that observed in the combined LARCS clusters ($d(B-R)/dr_p = -0.022 \pm 0.004$). The gradient in the CMR colour resulting from the variation in the morphological mix seen in the T–Σ relation is $d(B-R)/d\log_{10}(\Sigma) = 0.033$. This is equivalent to a change from $\log_{10}(\Sigma) > 2.5$ to $\log_{10}(\Sigma) = 0.0$ of $\Delta(B-R) = -0.10$, which is around 50 percent of that seen over this density range in the composite of the LARCS clusters ($d(B-R)/d\log_{10}(\Sigma) = -0.076 \pm 0.009$). We find similar predicted trends at 99 per cent confidence if we restrict ourselves to only the high L_X clusters from Dressler (1980).

5.2 Interpretation

Based on the results from the previous section we conclude that the morphology-radius and morphology-density relations seen in local clusters can account for only around half of the apparent change in galaxy colour with radius and local galaxy density seen in our sample.

We estimate therefore that there is an *intrinsic* gradient corrected for morphological differences in the colours of early-type galaxies at a fixed luminosity of $d(B-R)/d\log_{10}(\Sigma) = -0.011$ from the cores of typical rich clusters at $z \sim 0.12$ out to environments with galaxy densities of $\log_{10}(\Sigma) \sim 0$ (equivalent to a radius of 2 Mpc). The intrinsic variation with clustocentric radius gives a somewhat weaker trend (Table 5): $d(B-R)/dr_p = -0.005$.

Radial gradients in the colours of cluster galaxies have been previously reported by Abraham et al. (1996) and Terlevich et al. (2001) for two rich clusters straddling the redshift range studied here. These two measurements are not exactly comparable as the Terlevich et al. analysis focuses on the morphologically classified E and S0 galaxies, whereas Abraham et al. investigate a colour-selected sample around the CMR, similar to the approach used here. Nevertheless, as Terlevich et al. stress, the core of Coma is completely dominated by E and S0 galaxies and so their results would not change significantly if they considered the whole population.

Abraham et al. (1996) find radial gradient in $(g-r)$ colour of $d(g-r)/d\log_{10}(r_p) = -0.079$ out to 5 Mpc in A 2390 ($z = 0.23$), this is not corrected for any variations due to a $T-R$ relation. We estimate there is ~ 20 percent uncertainty in this gradient. Terlevich et al. (2001) report $d(g-r)/d\log_{10}(r_p) = -0.024 \pm 0.005$ for the Coma cluster, transformed to the same restframe wavebands as the observations A 2390. To compare our result with these we similarly transform the $(B-R)$ colours of galaxies in our composite $z = 0.12$ cluster to the wavelengths equivalent to observing a cluster in $(g-r)$ at $z = 0.23$. The result of this transformation is a radial gradient of $d(g-r)/d\log_{10}(r_p) = -0.061 \pm 0.011$ (uncorrected for the $T-R$ relation). Hence, the radial gradient of the colour of the CMR at $z = 0.12$ (a look-back time of 2 Gyrs) is intermediate between those found by Abraham et al. (1996) for A 2390 and Terlevich et al. (2001) for the Coma cluster at look-back times of 3.5 Gyr and 0.5 Gyrs respectively. Correcting the higher redshift measurements for the effects of the morphology-radius relation still results in steeper gradients at higher redshifts.

Both Abraham et al. (1996) and Terlevich et al. (2001) attribute the colour gradients they observe in the clusters to age trends (Terlevich et al. 2001 use detailed arguments to show that the variation in colour cannot be due to dust spread through the core of the cluster). Using the models for a single burst stellar population at an age of 7 Gyr (equivalent to the time elapsed between a formation epoch at $z \geq 2$ and $z = 0.12$) presented in Bower et al. (1998), we find $d(B-R)/dt \sim 0.03$ mag Gyr^{-1} (Kodama & Arimoto, 1997). This implies that the galaxies on the CMR in the outer regions of our clusters have luminosity-weighted stellar populations which are approximately 3 Gyrs younger than those in the cores ($r_p < 1$ Mpc). This age difference is comparable to that found by Terlevich et al. (2001) who predict that early-type galaxies in the outskirts of Coma have stellar pop-

ulations which are ~ 2 Gyr younger than those in galaxies in the central regions.

We also propose that the colour gradients observed in our sample represent variations in the ages of the stellar populations in the cluster galaxies arising from diffences in their star formation histories (Abraham et al. 1996; Smail et al. 1998, 2001; Kodama & Bower 2000). The bulk of galaxies on the CMR are expected to be S0's (Table 5; Dressler 1980; Fasano et al. 2001) and thus changes in the colours of this morphological class must play a major role in causing the observed colour gradient (Abraham et al. 1996). However, we also see evidence for a proportion of old, evolved galaxies whose colours are constant with environment and define the red wing of the CMR (Figure 7). We suggest that the majority of these galaxies are probably ellipticals, which show modest environmental variation in their properties (Treu et al. 1999). Thus a mix of ellipticals with constant colours and a dominant population of S0 galaxies, whose colours vary with environment, can reconcile the main results from our survey.

Why should galaxies which have S0 morphologies, or at least the colours of S0's at the present-day, vary with environment? Although still controversial, there is increasing evidence that the S0 population in rich clusters has come into being relatively recently. The proportion of S0 galaxies in rich clusters appears to increase rapidly to the present-day (Dressler et al. 1997; Fasano et al. 2001), possibly as the result of the transformation of star-forming disk galaxies which are accreted by the clusters from the surrounding field (Poggianti et al. 1999; Kodama & Smail 2001). The fact that we can see differences in the properties of cluster galaxies out at least as far as 6 Mpc from the cluster core suggests that the process which may suppress the star formation of infalling galaxies can operate in low density environments (Fasano et al. 2000; Bekki et al. 2001; Carlberg et al. 2001; Couch et al. 2001; Kodama et al. 2001). One mechanism for causing this transformation is the suppression of star formation due to the removal of the gas reservoirs as galaxies enter the cluster (Poggianti et al. 1999; Balogh, Navarro & Morris 2000). This mechanism may lead directly to the formation of an S0, or other processes may be involved (Balogh et al. 2001).

If this scenario is correct then the accretion and transformation of spiral galaxies from the surrounding field will lead to a gradual build-up of the S0 population within the cluster. Some morphological studies of the early-type galaxies in cluster cores at $z \sim 0.5$ imply that the majority of the S0 population in these regions today are transformed in the 6 Gyrs between $z = 0.5$ and the present-day (e.g. Poggianti et al. 1999). On the outskirts of the clusters we expect a higher proportion of recently arrived cluster members, reflecting the accretion history of the cluster (Abraham et al. 1996). Thus the S0 galaxies in these regions will show the strongest signatures of their past star formation activity, exhibiting the youngest luminosity-weighted ages for their stellar populations and hence the bluest colours. These two effects will combine to produce a radial colour gradient in the same sense as that seen in our data. After accounting for the varying morphological mix with environment, it appears that galaxies on the outskirts of these clusters have luminosity-weighted ages which are ~ 3 Gyrs younger than those in the core. It would be interesting to quantitatively compare this observation with theoretical predictions to test models for the infall history and transformation of galaxies in high density environments (Diaferio et al. 2001).

5.3 Caveats

Our analysis and interpretation is based upon a number of assumptions that require consideration and should be improved upon in future work. Perhaps the largest source of uncertainty is the background subtraction method employed. It is apparent from Figure 1 that there are a number of galaxies, which are rejected by the background subtraction algorithm, but which lie within the CMR (e.g. Abell 1650). Conversely, there must also be galaxies which are defined as cluster members, but which are in all likelihood interlopers. We re-emphasize that the background correction is purely a statistical method. There are two clear ways in which this method could be improved. Firstly, we could use a larger sample of dedicated field observations to improve the statistics. Secondly, we could use spectroscopic observations of the clusters to provide a more robust method to determine cluster membership.

During our analysis we combine our clusters into a single composite cluster to examine the radial dependance of the CMR. We note that the richer clusters (i.e. Abell 550, 1285 and 3888) have a greater weight in the composite cluster than the poorer ones (i.e. Abell 1079, 1084 and 1664). Although cluster-to-cluster variations are present within our sample, we emphasize that LARCS represents a homogeneously X-ray selected sample of clusters and therefore such cluster-to-cluster variations should be minimized. Using more clusters to create the combined cluster would be beneficial.

In our discussion we compare our data to that of Dressler (1980) to remove the $T - \Sigma$ relation from our clusters. We note that the LARCS dataset does not contain sufficiently high resolution imaging required morphologically classify galaxies. Hence we are unable to derive a $T - \Sigma$ relation for our clusters and we rely upon the morphology-density analysis performed by Dressler (1980) for other clusters. In using these data, we note that the Dressler (1980) sample is constructed with an inhomogeneous local ($z < 0.06$) sample of clusters and may, therefore, not be directly comparable to our study (although limiting Dressler's sample only to high L_X clusters gives the same results). To remedy this situation would require sub-arcsecond panoramic imaging of our clusters to provide the necessary morphological information.

6 CONCLUSIONS

We have analysed eleven clusters with precise photometric observations from the LARCS survey to trace the variation in the colours of evolved galaxies into the environmental transition region between clusters and the field.

- All of the clusters show colour-magnitude relations; many of these are strong and can be traced well beyond the central 1 Mpc, out to unprecedented clustocentric radii coverage of ~ 8 Mpc.

• We find that the characteristic colour and slope of the CMR of galaxies in the cluster cores change with cluster redshift across the range $z = 0.07$–0.16 covered by our sample. The variations in the CMRs are compatible with those expected from galaxy populations which formed the bulk of their stars at high redshifts, $z \gg 2$.

• The majority of clusters in the survey exhibit a variation with radius in the colour of the CMR at a fixed luminosity. When combined into a single composite cluster, we observe a radial colour gradient of $d(B-R)/dr_p = -0.022 \pm 0.004$ from the cluster centre to ~ 6 Mpc.

• The composite cluster formed from our sample also shows a colour-local-density relation for the galaxies on the CMR. We identify a colour gradient in the modal colours of galaxies on the CMR amounting to $d(B-R)/d\log_{10}(\Sigma) = -0.076 \pm 0.009$ across three orders of magnitude in local galaxy density from the high-density core of the cluster to the outskirts.

• We calculate the expected change in the colour of the CMR with environment due to the changing morphological mix. We estimate that approximately 50 to 70 per cent of the radial and density colour gradient is due to an increase in contamination by quiescent, early-type spiral galaxies falling close to the CMR. We suggest that the CMR consists of a passively evolving population (elliptical and evolved S0 galaxies) plus recent additions (morphologically young S0 and recently star-forming spiral galaxies).

• Our analysis of eleven clusters supports the previous claims of radial colour variations in individual rich clusters at $z = 0$ and $z = 0.23$. We have also shown that similar trends are visible when using local galaxy density as a more general measure of galaxy environment. Taken together with previous studies, we suggest that these environmental trends in the colours of galaxies at a fixed luminosity most likely reflect differences in the luminosity-weighted ages of the galaxies in different environments. If interpreted purely as a difference in ages and accounting for differences in the morphological mix, then the gradient observed in our sample suggests that the luminosity-weighted ages of the dominant galaxy population within the CMR at 6 Mpc from the cluster core are $\sim$3 Gyrs younger than those residing in the core.

• The results of our photometric analysis can provide a readily testable, quantitative prediction. If the observed colour gradient simply reflects age differences in passive stellar populations then we would expect that the typical $H\delta_A + H\gamma_A$ line strength of galaxies lying on the CMR should increase by ~ 4Å when moving from the cluster core to the outskirts of these systems (Terlevich et al. 1999).

• Further studies are urgently needed to investigate the properties of galaxies in the lower density environments which connect rich clusters to the surrounding field, particularly at higher redshifts. This region is essential for investigating the impact of environment upon the star formation and morphologies of galaxies.

This is the second paper in a series based upon the LARCS survey. In the next paper we will examine 2dF spectroscopy for several of the clusters from the survey (O'Hely et al. in prep.).

Acknowledgements

We thank Richard Bower and Peter S. Craig for insightful and stimulating discussions. We also thank Michael Balogh, Ray Sharples and Simon Morris for their careful reading of this manuscipt and providing many useful suggestions which have improved this work. KAP acknowledges support from his PPARC studentship. IRS acknowledges support from the Royal Society and a Philip Leverhulme Prize Fellowship. TK acknowledges the Japan Society for Promotion of Science through its Research Fellowships for Young Scientists. WJC and EO'H acknowledge the financial support of the Australian Research Council. ACE acknowledges support from the Royal Society. AIZ acknowledges support from NASA grant HF-01087.01-96. We thank the Observatories of the Carnegie Institution of Washington for their generous support of this survey. This research has made extensive use of the University of Durham's STARLINK computing facilities, expertly managed by Alan Lotts, and the facilities at Las Campanas Observatory, Chile.

REFERENCES

Abraham, R. G., Smecker-Hane, T. A., Hutchings, J. B., Carlberg, R. G., Yee, H. K. C., Ellingson, E., Morris, S. L., Oke, J. B., Rigler, M., 1996, ApJ, 471, 694.
Abraham R. G., Valdes F., Yee H. K. C., van den Bergh S., 1994, ApJ, 432, 75
Andreon, S. 1998, ApJ, 501, 533
Babul, A., Balogh, L. M., Lewis, G. F., & Poole, G. B. 2001, MNRAS, submitted
Balogh, M. L., Navarro, J. F. & Morris, S. L. 2000, ApJ, 540, 113
Balogh, M. L., Morris, S. L., Yee, H. K. C., Carlberg, R. G. & Ellingson, E. 1999, ApJ, 527, 54
Beers, T. C., Flynn, K., & Gebhardt, K. 1990, AJ, 100, 32
Bekki, K., Couch, W. J., & Shioya, Y. 2001, PASJ, 53, 395
Bertin, E. & Arnouts, S. 1996, A&AS, 117, 393
Bower, R. G., Kodama, T., & Terlevich, A. 1998, MNRAS, 299, 1193
Bower, R. G., Lucey, J. R. & Ellis, R. S. 1992, MNRAS, 254, 601
Butcher, H. & Oemler, A. 1984, ApJ, 285, 426
Butcher, H. & Oemler, A. 1978, ApJ, 226, 559
Caldwell, N., Rose, J. A., Sharples, R. M., Ellis, R. S., & Bower, R. G. 1993, AJ, 106, 473
Carlberg, R. G., Yee, H. K. C., Morris, S. L., Lin, H., Hall, P. B., Patton, D. R., Sawicki, M., & Shepherd, C. W. 2001, ApJ, 552, 427
Carlberg, R. G., Yee, H. K. C., Ellingson, E., Abraham, R., Gravel, P., Morris, S., & Pritchet, C. J. 1996, ApJ, 462, 32
Cole, S., Lacey, C. G., Baugh, C. M., & Frenk, C. S. 2000, MNRAS, 319, 168
Couch, W. J., Balogh, M. L., Bower, R. G., Smail, I., Glazebrook, K., & Taylor, M. 2001, ApJ, 549, 820
Couch, W. J., Barger, A. J., Smail, I., Ellis, R. S. & Sharples, R. M. 1998, ApJ, 497, 188
Couch, W. J. & Sharples, R. M. 1987, MNRAS, 229, 423
de Vaucouleurs, G., de Vaucouleurs, A., Corwin, H. G., Buta, R. J., Paturel, G., & Fouque, P. 1991, Volume 1-3, XII, 2069 pp. 7 figs.. Springer-Verlag Berlin Heidelberg New York
Diaferio, A., Kauffmann, G., Balogh, M. L., White, S. D. M., Schade, D., & Ellingson, E. 2001, MNRAS, 323, 999
Dressler, A., Smail, I., Poggianti, B. M., Butcher, H., Couch, W. J., Ellis, R. S. & Oemler, A. J. 1999, ApJS, 122, 51
Dressler, A. et al. 1997, ApJ, 490, 577
Dressler, A. 1984, ApJ, 281, 512

Dressler, A. 1980, ApJ, 236, 351
Ebeling, H., Voges, W., Bohringer, H., Edge, A. C., Huchra, J. P. & Briel, U. G. 1996, MNRAS, 281, 799 (XBACS)
Ellis, R. S., Smail, I., Dressler, A., Couch, W. J., Oemler, A. J., Butcher, H. & Sharples, R. M. 1997, ApJ, 483, 582
Fasano, G., Poggianti, B. M., Couch, W. J., Bettoni, D., Kjærgaard, P., & Moles, M. 2000, ApJ, 542, 673
Fasano, G. & Franceschini, A. 1987, MNRAS, 225, 155
Glazebrook K., Peacock J.A., Collins, C.A., Miller L., 1994, MNRAS, 266, 65
King, C. R. & Ellis, R. S. 1985, ApJ, 288, 456
Kodama, T. & Arimoto, N. 1997, A&A, 320, 41
Kodama, T., Bower, R. G., 2001, MNRAS, 321, 18
Kodama, T., Bower, R. G., Bell, E.F., 1999, MNRAS, 306, 561
Kodama, T., Smail, I., Nakata, F., Okamura, S. & Bower, R. G., 2001, ApJL, in press
Lacey, C. & Cole, S. 1993, MNRAS, 262, 627
Landolt, A. U. 1992, AJ, 104, 340
Larson, R. B., Tinsley, B. M., & Caldwell, C. N. 1980, ApJ, 237, 692
Lubin, L. M., Postman, M., Oke, J. B., Ratnatunga, K. U., Gunn, J. E., Hoessel, J. G., & Schneider, D. P. 1998, AJ, 116, 584
Metcalfe, N., Shanks, T., Fong, R., & Jones, L. R. 1991, MNRAS, 249, 498
O'Hely, E., Ph.D. Thesis "Bridging the gap", UNSW, 2000.
O'Hely, E., Couch, W.J., Smail, I., Edge, A.C., Zabludoff, A., 1998, PASA, 15, 3, 27
Pimbblet, K. A., Smail, I., Edge, A. C., Couch, W. J., O'Hely, E., & Zabludoff, A. I. 2001, MNRAS, 327, 588
Poggianti, B. M., Smail, I., Dressler, A., Couch, W. J., Barger, A. J., Butcher, H., Ellis, R. S., & Oemler, A. J. 1999, ApJ, 518, 576
Press, W. H., Teukolsky, S. A., Vetterling, W. T., & Flannery, B. P. 1992, Cambridge: University Press, —c1992, 2nd ed.
Roberts, M. S. & Haynes, M. P. 1994, ARA&A, 32, 115
Sandage, A., Freeman, K. C., & Stokes, N. R. 1970, ApJ, 160, 831
Schlegel D.J., Finkbeiner D.P., Davis M., 1998, ApJ, 500, 525
Smail, I., Kuntschner, H., Kodama, T., Smith, G. P., Packham, C., Fruchter, A. S. & Hook, R. N., 2001, MNRAS, 323, 839-849
Smail, I., Edge, A.C., Ellis, R.S., Blandford, R.D., 1998, MNRAS, 293, 124-144
Terlevich, A. I., Caldwell, N. & Bower, R. G. 2001, MNRAS, 326, 1547
Terlevich, A. I., Kuntschner, H., Bower, R. G., Caldwell, N., & Sharples, R. M. 1999, MNRAS, 310, 445
Terlevich, A. I., 1998, Ph.D. Thesis, University of Durham
Treu, T., Stiavelli, M., Casertano, S., Møller, P., & Bertin, G. 1999, MNRAS, 308, 1037
van Dokkum, P. G., Franx, M., Fabricant, D., Illingworth, G. D., & Kelson, D. D. 2000, ApJ, 541, 95
van Dokkum, P. G., Franx, M., Illingworth, G. D., Kelson, D. D., Fisher, D., Fabricant, D., 1998, ApJ, 500, 714
Visvanathan, N., & Sandage, A., 1977, ApJ, 216, 214
Whitmore, B. C., Gilmore, D. M., & Jones, C. 1993, ApJ, 407, 489
Whitmore, B. C. & Gilmore, D. M. 1991, ApJ, 367, 64
Yee, H. K. C., Ellingson, E., & Carlberg, R. G. 1996, ApJS, 102, 269

APPENDIX A: STATISTICAL CORRECTION.

To examine the cluster galaxy population in the absence of spectroscopy, it is necessary to statistically subtract the field population from a given cluster plus field population. Typically, to obtain the cluster population one subtracts off an area and density-scaled portion of the defined field population, $F_{\rm pop}$, from the defined cluster plus field population, $C + F_{\rm pop}$. Both the $F_{\rm pop}$ and the $C + F_{\rm pop}$ are then binned onto a sensibly gridded colour-magnitude diagram. A straight forward subtraction is then performed to calculate the probability of a galaxy in a given colour-magnitude grid position of being a field galaxy. Thus:

$$P(\mathrm{Field})_{\rm col,mag} = \frac{\mathrm{N(Field)_{col,mag}} \times \mathrm{A}}{\mathrm{N(Cluster + Field)_{col,mag}}} \qquad (1)$$

where A is an area- and density-dependant scaling factor. For each galaxy in $C + F_{\rm pop}$, we proceed to generate a random number between 0.0 and 1.0 and compare it to the galaxies' value of $P(\mathrm{Field})_{\rm col,mag}$ in order to determine if the given galaxy should be in the resultant cluster population. Problems in this method occur when directly subtracting the populations on the color-magnitude plane produces a negative number of galaxies in the cluster population, $C_{\rm popn}$, for a particular grid position. A resultant $P(\mathrm{Field})_{\rm col,mag}$ can thus be greater than 1.0. Therefore to utilize a background subtraction method to analyze a cluster population in the absence of spectroscopy, it is necessary to solve this "negative galaxy" problem. A typical method is to normalize all of the probabilities to the largest value of $P(\mathrm{Field})_{\rm col,mag}$. Clearly such a solution has drawbacks as the resultant $P(\mathrm{Field})_{\rm col,mag}$ distribution no longer reflects the appropriately scaled input data and has actually been scaled away from its true value in many locations on the color-magnitude plane for the sake of one (or a few) anomalously low counts in $C + F_{\rm pop}$ for a particular grid position.

The method adopted in this study is similar to that used by Smail et al. (1998) and Kodama & Bower (2001, KB01). If, when gridding up the colour-magnitude diagrams, we produce a negative galaxy in the computation of $P(\mathrm{Field})_{\rm col,mag}$, we solve it by increasing the grid size *for that particular grid position*. Thus the grid position $(\mathrm{col}, \mathrm{mag})$ is increased to include its nearest neighbours $(\mathrm{col} : \mathrm{col}+1, \mathrm{mag} : \mathrm{mag}+1)$ and then $P(\mathrm{Field})_{\rm col,mag}$ is recalculated using this new 2×2 grid. If this is not enough to cure the negative galaxy problem, we increase the grid size for that particular grid position by one further step to $(\mathrm{col}-1 : \mathrm{col}+1, \mathrm{mag}-1 : \mathrm{mag}+1)$ and so on until the field-corrected galaxy count exceeds zero.

In Figure 8 we compare the resultant $P(\mathrm{Field})_{\rm col,mag}$ distribution using this method and KB01. The grid position $(3, 2)$ has a fluctuation in $C + F_{\rm pop}$ so that the number of galaxies in the corresponding grid position in $F_{\rm pop}$ makes the resultant $P(\mathrm{Field})_{3,2} > 1.0$. By normalizing to the anomalous value, *all* the rest of the probabilities are reduced from their original values and we are still left with a high probability at the original grid position. The KB01 method subtracts the excess probability (in this case 0.2) and distributes it evenly between its neighbours, making the original grid position $P(\mathrm{Field})_{3,2} = 1.0$. Using our new method, we resample grid positions $(3:4, 2:3)$ to make one new, larger grid position and calculate the new probability for this.

It is found that the negative galaxy problem exists in all clusters examined in this study. The number of grid-expansions required to cure the problem are typically around ten 2×2 expansions and a small number of larger order

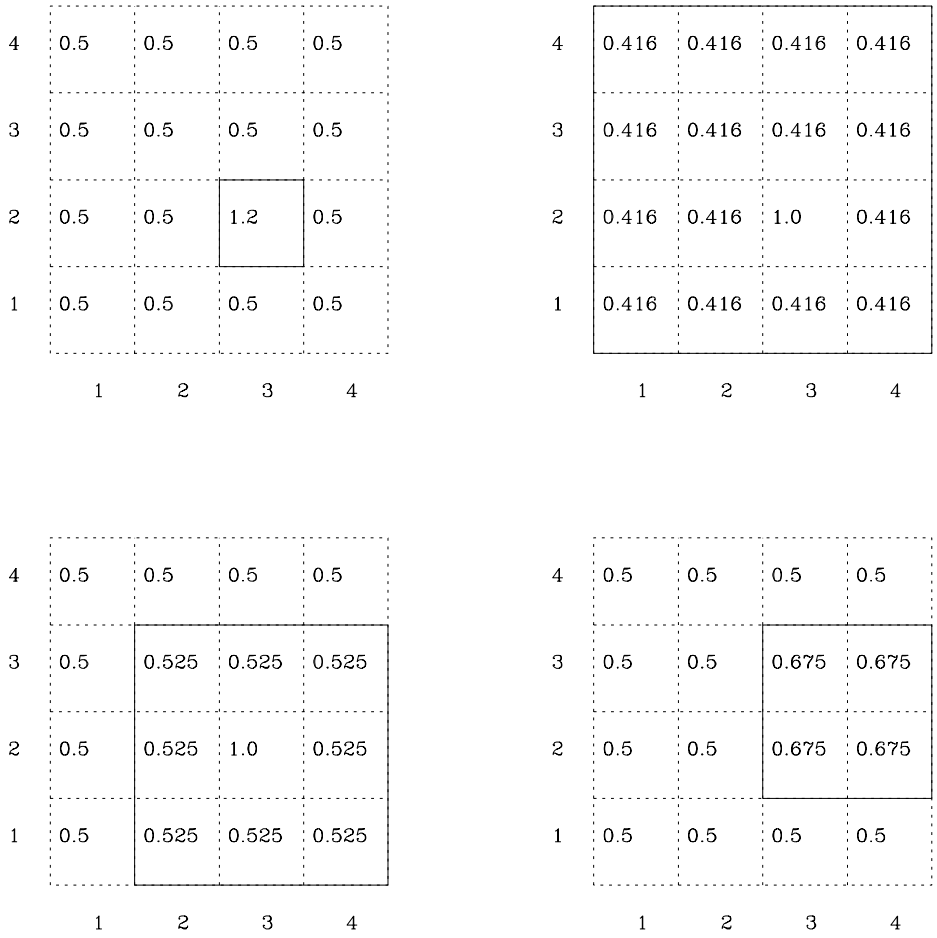

Figure 8. A comparison of the statistical correction methods on the colour-magnitude plane. The galaxies have been binned into a colour-magnitude grid and the calculated P(Field) is shown for each grid position. [top left]: An example distribution of P(Field) containing a grid position with P(Field) > 1.0 – the negative galaxy problem. [top right]: Normalizing *all* the points to the anomalous grid position retains the original anomalous point and artificially decreases the probabilities in the remainder of the grid. [bottom left]: The approach used by KB01: the excess 0.2 probability is distributed equally into neighbouring grid cells. [bottom right]: Adaptive-mesh method used in this work – the lowest possible number of grid positions are used to recalculate the P(Field) distribution and no obvious fluctuation remains.

expansions. The expansions are typically situated away from the CMR, preferentially where the $C + F_{\rm pop}$ is sparse.

As with all background subtraction methods, this technique has advantages and drawbacks. Whilst it preserves the original probability distributions better than other methods, it also has a tendency to "smear" the resultant distribution. To illustrate this one can imagine a situation where one grid position has a P(Field) > 1 whilst its neighbours have very small values of P(Field). Upon expansion of the grid, the probabilities of being a field galaxy significantly increase for those grid positions that initially had a very low P(Field). Therefore we effectively remove galaxies from adjoining grid positions to make up for the one grid position which had P(Field) > 1. It is because of this that we may expect that statistics on sparsely populated areas of a colour-magnitude diagram to be adversely affected (e.g. it is likely that the blue population, and hence f_B, is underestimated). Unlike previous methods, this new technique minimizes the number of grid positions affected in this manner.